Trends in Atmospheric Sci., 1 (1992)

Dynamics of thermally forced mesoscale circulations

Yuh-Lang Lin
Department of Marine, Earth, and Atmospheric Sciences, North Carolina State University Raleigh, North Carolina 27695-8208, USA.

1. Introduction

There are a number of problems in mesoscale dynamics which are related to the response of a stably stratified flow to localized heat sources or sinks. A phenomenon is defined as mesoscale if it has a horizontal scale of 2 to 2000 km. The mesoscale is often divided into three subscales: meso-γ (2-20 km), meso-β (20-200 km), and meso-α (200-2000 km) scales (Orlanski, 1975). In some cases, the diabatic heating or cooling reaches a quasi-steady state, which may be represented by a prescribed function. In this way, the mathematical problem reduces to a stably stratified flow over a prescribed thermal forcing. Some examples will be briefly reviewed below to demonstrate that this type of study is useful in understanding the dynamics of different types of mesoscale phenomena spanning the various subscales.

One of the earliest theoretical studies of airflow over a prescribed heat source was proposed by Malkus and Stern (1953) in a study of the heat island problem. They found that the air ascends over the heat island. As pointed out by Olfe and Lee (1971) and Smith and Lin (1982), this is not the case if a correct upper boundary condition is imposed. Observations over heat islands such as Anegada (Malkus, 1963) and Barbados (Fig. 25; DeSouza, 1972; summarized in Garstang et al., 1975) showed that there exists a region of descent over the heat island followed by an ascent over the ocean on the downwind side during the daytime. By solving an associated transient problem, Lin and Smith (1986) also suggested that the rainfall enhancement occuring on the downwind side of an urban heat island, such as St. Louis (Fig. 1; Braham and Dungey, 1978; Changnon, 1981), may be partly the result of the ascent produced by the stationary heating due to the urban heat island. This problem has also been studied by several authors (e.g. Smith, 1955, 1957; Hsu, 1987a,b; Luthi et al., 1989). Circulations associated with sea/land breezes are also related to this process except that the thermal forcing is periodic in time. Since the sea breeze problem has been studied extensively in the last four decades and is reviewed in several textbooks and literature articles (e.g., Rotunno, 1983), we will not review this subject in this paper.

In a study of the upslope orographic rain problem, Smith and Lin (1982) solved the mathematical problem analytically using a prescribed function to represent the latent heating associated with the nonprecipitating or precipitating orographic cloud in a stably stratified flow. They found that the phase relationship between the heating and the induced vertical displacement is negative in a moving airstream. That is, descending motion is established

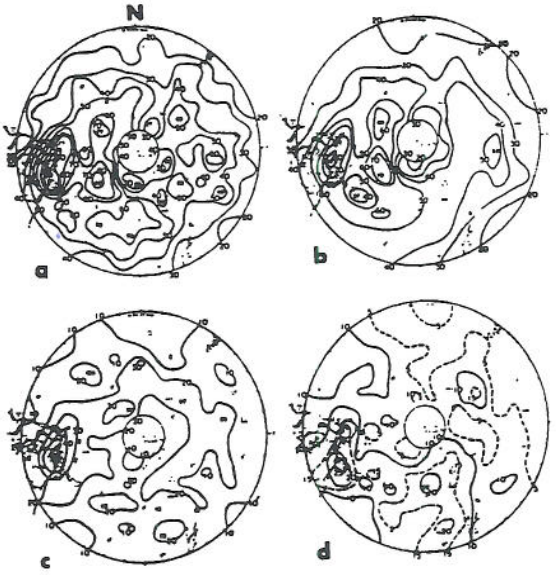

Fig. 1: Maps of first echo densities in St. Louis, Mo.: (a) analysis of 4553 first echoes, (b) set of 4175 first echoes having bases ≥ 3000 ft, (c) set of 1950 echoes from 44 days selected to insure ground based convective clouds, (d) data for days with light wind. Downtown St. Louis is denoted by X. Notice that the first echo formation is on the downwind region of the city. (From Braham and Dungey, 1978)

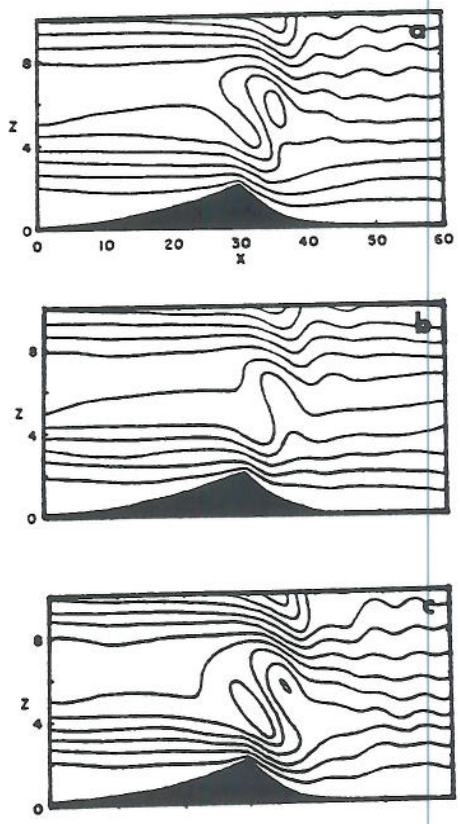

Fig. 2: Airflow over a ridge: (a) adiabatic, (b) with boundary layer heating, and (c) with boundary layer cooling. Notice that the adiabatic mountain waves are suppressed by the heating and enhanced by the cooling (From Raymond, 1972)

just upstream of the prescribed heated region so that negative displacements dominate in the heating region. This phenomenon is consistent with other studies of the orographic rain problem (e.g., Fraser et al., 1973; Barcilon et al., 1980) in which it was found that the mountain waves are weakened by the latent heating. Raymond (1972) also showed that mountain waves are weakened by heating and strengthened by cooling in a study of airflow over a two-dimensional ridge with low-level sensible heating and cooling (see Fig. 2). This phenomenon was then explained by Lin and Smith (1986) by solving the transient problem and by Bretherton (1988) by proposing a group velocity argument. The combined effect of thermal and orographic forcing has also been studied by Davies and Schar (1986). In their theory, they incorporated a CISK-like representation for a non-precipitating convective cloud in a linear, steady, continuously stratified, hydrostatic flow over a mountain ridge. They found that the effect of combined thermal and orographic forcing can be significantly different from that of orography acting alone. In particular, in certain

situations an enhanced (resonant) response can occur with strong winds on the lee slope and a concomitant large surface pressure drag. Their results also suggested that diabatic effects might on occasion play a major role in inducing strong surface leeside winds.

The response of a continuously stratified atmosphere to diabatic forcing is also relevant to the moist convection associated with midlatitude squall lines. One may regard the evaporative cooling in the subcloud layer produced by the precipitation falling from the updraft aloft as a stationary heat sink in the reference frame of the moving line. The steady state assumption for the cooling in squall-line type thunderstorms is not an unreasonable one (Lilly, 1979). The mathematical problem has been investigated by several authors (Thorpe et al., 1980; Lin and Smith, 1986; Raymond and Rotunno, 1989; Lin and Chun, 1991). The solutions provide a way to help explain the maintenance of a long lasting squall line. In solving a similar two-dimensional initial value problem with both prescribed condensational heating and evaporative cooling considered, Raymond (1986) indicated that the strong speed selectivity of wave-CISK is due to a requirement that the actual vertical velocity at the level of free convection must exceed the diabatic mass flux there. In solving the three-dimensional response to a prescribed elevated heating, representing condensational heating, Lin (1986a) and Lin and Li (1988) proposed that the V-shaped cloud tops over severe storms (Fig. 3; also see Heymsfield and Blackmer, 1988 for a brief review) are formed by thermally forced gravity waves. By incorporating a prescribed elevated cooling associated with melting snow, it has been shown that new convection may be triggered (Lin, C.A. et al., 1988a,b).

Occasionally, there exists a critical level in a flow over a heat source or sink. One example is the moist convection associated with midlatitude squall lines (e.g., Thorpe et al., 1982; Seitter and Kuo, 1983; Raymond, 1984). For the squall line analyzed by Ogura and Liou (1980), the rightward mode exhibits a critical level near 6 km (Fig. 4). That is, the propagation speed of the disturbance coincides with the environmental wind speed at that level. Similar phenomena have also been found in climatological studies by Bluestein and Jain (1985; see Fig. 5) and Wyss and Emanuel (1988). Thus, there exists thermal forcing below and above the critical level as the condensational heating may extend to a height of 10 km. Notice that the critical level coincides with the level of wind reversal in a steady state flow. Similar processes can also be found for moist southwesterly monsoon currents over the Western Ghats of India during the summer (Fig. 16 and 17; Ramage, 1971; Smith and Lin, 1983). Perpendicular to the coast line, the basic flow reverses in the middle troposphere.

In some cases, the thermal forcing exists solely below the critical level. For example, this problem is relevant to the formation of a squall line in the vicinity of a dry line over the southern Great Plains (Rhea, 1966). The mesoscale circulation across the dry line favorable for the formation and maintenance of a squall line analyzed by Ogura and Chen (1977) and simulated by Sun and Ogura (1979) appears to have a wind reversal near a low-level inversion (e.g., see Figs. 6c and 10b in Sun and Ogura). Sun and Ogura also found that upward motion is generated with sufficient intensity to release the potential instability if the synoptic-scale low-level wind is incident from the proper direction. Numerical studies of the sea breeze circulation (e.g., Estoque, 1962) also indicate that the location and shape as well as the intensity of the sea breeze circulation are

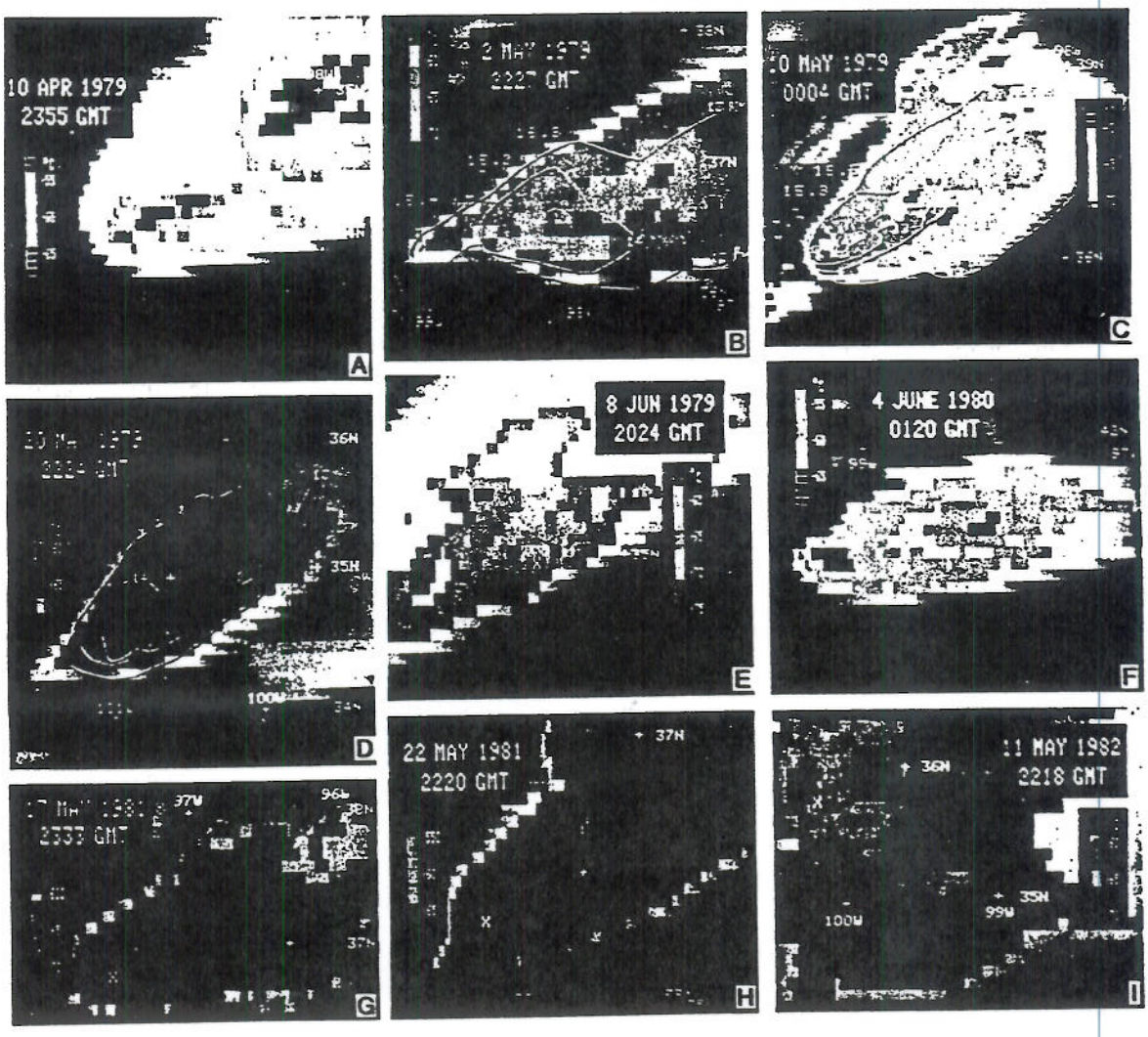

FIG. 3 IR GOES images. Stereo height contours are shown when available; an X indicates approximate cloud top position as obtained from visible image. Note color temperature assignments are not consistent between images.

strongly affected by the direction of the prevailing synoptic wind. Therefore, it is important to investigate the response of a continuously stratified shear flow with a critical level to prescribed heating or cooling.

The above mentioned problem may be further applied to the mesoscale flow in the vicinity of the coastal region of the Carolinas during the winter when a cold synoptic-scale anticyclone exists to the north of this region. The horizontal basic wind normal to the coastline reverses at about 2 km as the inland low-tropospheric flow underlies the westerlies in the middle and upper troposphere (Fig. 6). The low-level sensible and latent heating associated with the strong temperature contrast provides an important energy source for the mesoscale circulation, which can produce a subsynoptic scale cyclone near the surface (Lin, 1989b, 1990a). Since the Rossby

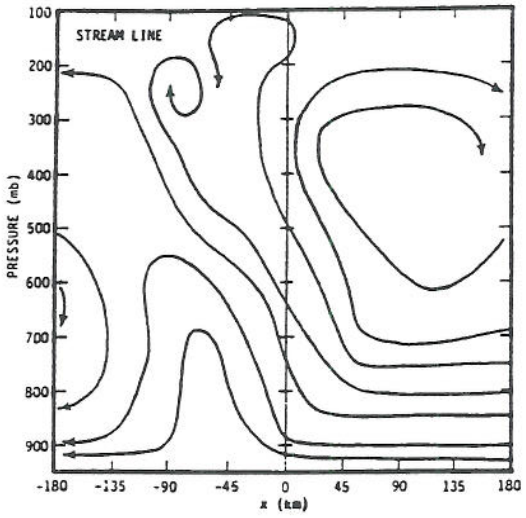

Fig. 4: Streamlines for a midlatitude squll line on 22 May 1976. Three important features are shown: (a) upshear tilt of the updraft, (b) downdraft fed by the front-to-rear flow, and (c) flow overturning in the middle layer (From Ogura and Liou, 1980)

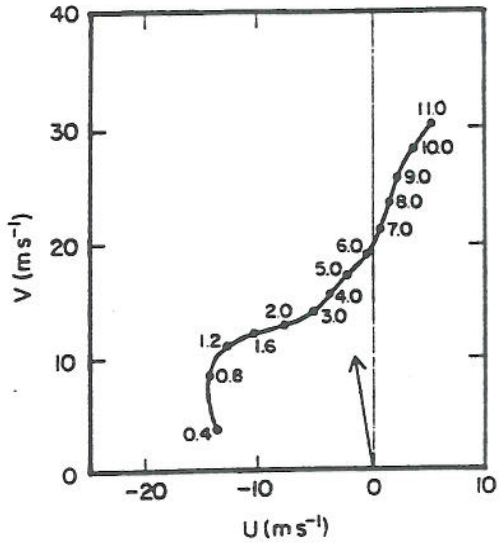

Fig. 5: Composite hodographs in a frame of reference moving along with squall lines averaged over an 11 year period in Oklahoma. (From Bluestein and Jain, 1985)

number associated with the flow is less than one, the response is quite different from that of a stratified flow over a small-scale heat source with rotational effects ignored. Therefore, in order to understand the dynamics of a flow over a meso-α/β scale heat source, the effects of planetary rotation as well as the baroclinicity must be included.

Prescribed diabatic heating in a large-scale atmospheric flow has also been found to be useful in understanding and interpreting the large scale dynamics. For example, Smagorinsky (1953) has investigated the large-scale steady flow over prescribed sinusoidal heat sources and sinks on a β-plane. The linear response of a large scale flow over steady tropical thermal forcing has also been studied extensively by several authors (e.g., Webster, 1972; Gill, 1980; Geisler, 1981; Geisler and Stevens, 1982; DeMaria, 1985). The Walker circulation results from the dominance of the convective heating of the Indonesian maritime continent. The midlatitude response to steady tropical thermal forcing has been studied by Hoskins and Karoly (1981), Simmons (1982), Lim and Chang (1983) among others. These studies showed that the uniform zonal flow, as well as the shear zonal flow (Lau and Lim, 1984), has a large effect on the midlatitude response to the imposed thermal forcing. However, we will concentrate on the application to mesoscale circulations in this review.

Therefore, the mathematical problem of prescribed diabatic heating in a continuously stratified flow has been shown to be useful in understanding the dynamics of various mesoscale phenomena which commonly occur in the terrestrial atmosphere by the above authors and by others. This subject has been reviewed recently by C. A. Lin and Stewart (1991). However, we will review a wider variety of problems and emphasize more on

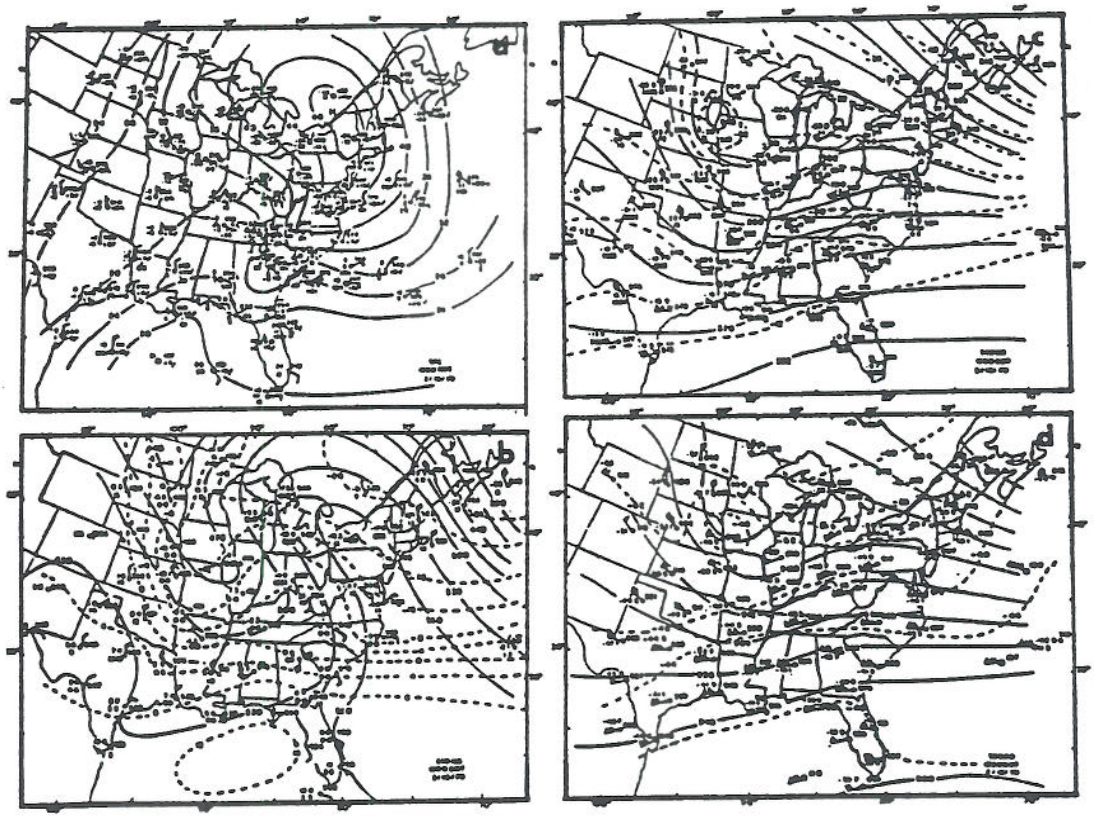

Fig.6: (a) Surface, (b) 850, (c) 500 and (d) 300 mb maps for 1200 GMT 18 February Presidents' Day snowstorm. Wind in m s^{-1} [pennant=25 m s^{-1}, full bar=5 m s^{-1}], temperature in °C. Heights, surface pressures and isotherms indicated by solid and dashed lines, respectively. (From Bosart, 1981)

the basic dynamics. The governing equations for a mesoscale atmospheric system will be presented in Section 2. An energy equation will be used to identify various instability mechanisms. A dispersion relation will be derived and used to categorize different wave regimes. Finally, the wave reflection and effect of critical level will be discussed. In Section 3, the response of a uniform, steady, continuously stratified flow over a meso-γ scale heat source or sink will be described. Both sinusoidal and isolated heat sources will be considered. Applications to the orographic rain problem will be discussed. In Section 4, the transient flow response to a meso-γ scale heat source will be reviewed. Both pulse heating and steady heating will be included. Applications to the mesoscale circulations induced by orographic rain, heat islands, moist convection and gravity waves on inversions will be reviewed. In Section 5, the response of a continuously stratified shear flow with a critical level to a meso-γ scale heat source will be described. Responses to both heating and cooling will be included. The response of a three-dimensional flow to a prescribed local heating will be

described and applied to the dynamics of V-shaped cloud tops over severe storms. In Section 6, we will review the response of a flow over a meso-α/β scale heat source. The effects of planetary rotation will be included in this section. Responses to both barotropic and baroclinic flows will be discussed. The theory will then be applied to the problem of coastal cyclogenesis.

2. Governing Equations of Mesoscale Systems

Consider an inviscid, incompressible atmosphere on a planetary f-plane. The momentum equations, the incompressible continuity equation, and the thermodynamic energy equation can be expressed in the form

$$\frac{Du}{Dt} - fv + \frac{1}{\rho}\frac{\partial p}{\partial x} = 0 \tag{2.1}$$

$$\frac{Dv}{Dt} + fu + \frac{1}{\rho}\frac{\partial p}{\partial y} = 0 \tag{2.2}$$

$$\frac{Dw}{Dt} + g + \frac{1}{\rho}\frac{\partial p}{\partial z} = 0 \tag{2.3}$$

$$\frac{\partial u}{\partial x} + \frac{\partial v}{\partial y} + \frac{\partial w}{\partial z} = 0 \tag{2.4}$$

$$\frac{D\theta}{Dt} = \frac{\theta_o}{c_p T_o} q . \tag{2.5}$$

The diabatic heating rate per unit mass, q, may be taken to represent the surface heating and/or the elevated latent heating. The symbols θ_o and T_o denote constant reference potential temperature and temperature, respectively. Other symbols are defined as usual. Notice that the Rayleigh friction and Newtonian cooling may be included to generalize the above system. Since we have assumed an incompressible atmosphere, the physical mechanism responsible for generation and subsequent propagation of sound (acoustic) waves has been eliminated from the system.

We may linearize the above system by defining

$$\begin{aligned} u(t,x,y,z) &= U(z) + u'(t,x,y,z) \\ v(t,x,y,z) &= V(z) + v'(t,x,y,z) \\ w(t,x,y,z) &= \quad\; w'(t,x,y,z) \\ \rho(t,x,y,z) &= \rho_o + \rho'(t,x,y,z) \\ p(t,x,y,z) &= P(x,y,z) + p'(t,x,y,z) \\ \theta(t,x,y,z) &= \Theta(x,y,z) + \theta'(t,x,y,z) \\ q(t,x,y,z) &= \quad\; q'(t,x,y,z). \end{aligned} \tag{2.6}$$

In the above expressions, the Boussinesq approximation (Spiegel and Veronis, 1960) has been adopted, which assumes the density to be constant except in the buoyancy term. The basic wind is constrained to be uniform in horizontal. The basic state momentum relations are assumed to satisfy the hydrostatic and geostrophic wind balance

$$\frac{\partial P}{\partial z} = \frac{g\rho_o}{\theta_o}\Theta \tag{2.7a}$$

$$U = \frac{-1}{f\rho_o}\frac{\partial P}{\partial y}, \qquad V = \frac{1}{f\rho_o}\frac{\partial P}{\partial x}. \tag{2.7b}$$

The above equations imply the existence of thermal wind balance for the basic state

$$\frac{\partial \Theta}{\partial x} = \frac{f\theta_o}{g} V_z, \qquad \frac{\partial \Theta}{\partial y} = -\frac{f\theta_o}{g} U_z. \tag{2.8}$$

Substituting Eq.(2.6) into Eqs.(2.1)-(2.5) and neglecting the nonlinear terms, the perturbation equations can be written

$$\frac{\partial u'}{\partial t} + U\frac{\partial u'}{\partial x} + V\frac{\partial u'}{\partial y} + U_z w' - fv' + \frac{1}{\rho_o}\frac{\partial p'}{\partial x} = 0 \tag{2.9}$$

$$\frac{\partial v'}{\partial t} + U\frac{\partial v'}{\partial x} + V\frac{\partial v'}{\partial y} + V_z w' + fu' + \frac{1}{\rho_o}\frac{\partial p'}{\partial y} = 0 \tag{2.10}$$

$$\frac{\partial w'}{\partial t} + U\frac{\partial w'}{\partial x} + V\frac{\partial w'}{\partial y} - g\frac{\theta'}{\theta_o} + \frac{1}{\rho_o}\frac{\partial p'}{\partial z} = 0 \tag{2.11}$$

$$\frac{\partial u'}{\partial x} + \frac{\partial v'}{\partial y} + \frac{\partial w'}{\partial z} = 0 \tag{2.12}$$

$$\frac{\partial \theta'}{\partial t} + U\frac{\partial \theta'}{\partial x} + V\frac{\partial \theta'}{\partial y} + \frac{f\theta_o}{g}(V_z u' - U_z v') + \frac{N^2\theta_o}{g} w' = \frac{\theta_o}{c_p T_o} q' \tag{2.13}$$

The Brunt-Vaisala frequency is defined as

$$N^2 = \frac{g}{\theta_o}\frac{\partial \Theta}{\partial z} . \tag{2.14}$$

and may be characterized as the natural oscillation frequency of an air parcel displaced from its equilibrium positions in a continuously stratified atmosphere.

Eqs. (2.9)-(2.13) can be combined to give a single equation for the vertical velocity

$$\frac{D}{Dt}\left\{\frac{D^2}{Dt^2}\nabla^2 w' + f^2 w'_{zz} - \left(U_{zz}\frac{D}{Dt} + f V_{zz}\right)w'_x - \left(V_{zz}\frac{D}{Dt} - f U_{zz}\right)w'_y + N^2\nabla_H^2 w' + 2f\left(U_z w'_{yz} - V_z w'_{xz}\right)\right\} + 2fU_z V_z(w'_{xx} - w'_{yy}) + 2f(V_z^2 - U_z^2)\cdot w'_{xy} - 2f^2\left(U_z w'_{xz} + V_z w'_{yz}\right) = \frac{g}{c_p T_o}\frac{D}{Dt}\nabla_H^2 q' \tag{2.15}$$

The above mesoscale system includes the following mechanisms: (a) inertia-gravity wave generation, (b) convective instability, (c) shear instability, (d) symmetric instability, and (e) baroclinic instability (Emanuel and Raymond, 1984).

The energy transfer equation for the system of Eqs. (2.9)-(2.13) with no north-south (meridional) basic state wind component (V=0), but one whose east-west (zonal) component is meridionally sheared ($U_y \neq 0$) can be derived

$$\left(\frac{\partial}{\partial t} + U\frac{\partial}{\partial x}\right)E + \rho_o u'w'U_z + \rho_o u'v'U_y - \frac{\rho_o g f}{N^2\theta_o}v'\theta'U_z + \nabla\cdot(p'V) = \left(\frac{\rho_o g^2}{c_p T_o N^2\theta_o}\right)\theta' q' \tag{2.16}$$

where

$$E = \frac{\rho_o}{2}\left[(u'^2 + v'^2 + w'^2) + \left(\frac{g}{N\theta_o}\right)^2 \theta'^2\right] \tag{2.17}$$

is the total perturbation energy which consists of the perturbation kinetic energy (first term) and the perturbation potential energy (second term). Taking the horizontal integration of Eq. (2.17) over a single wavelength for a periodic disturbance or from $-\infty$ to $+\infty$ for a localized disturbance in both x and y directions gives

$$\frac{\partial \overline{E}}{\partial t} = -\rho_o\overline{uw}U_z - \rho_o\overline{uv}U_y + \left(\frac{\rho_o g f}{N^2\theta_o}\right)\overline{v\theta}U_z - \frac{\partial}{\partial z}\overline{pw} + \left(\frac{\rho_o g^2}{c_p T_o N^2\theta_o}\right)\overline{\theta q} \tag{2.18}$$

Now we may take the vertical integration of the above equation from z=0 to the top of the physical domain $z=z_T$ in which we are interested, to yield

$$\frac{\partial E_T}{\partial t} = -\rho_o\int_o^{z_T}\overline{uw}U_z dz - \rho_o\int_o^{z_T}\overline{uv}U_y dz + \left(\frac{\rho_o g f}{N^2\theta_o}\right)\int_o^{z_T}\overline{v\theta}U_z dz - \overline{pw}(z_T) + \overline{pw}(0) + \left(\frac{\rho_o g^2}{c_p T_o N^2\theta_o}\right)\int_o^{z_T}\overline{\theta q}dz \tag{2.19}$$

The term on the left side of the above equation represents the time rate of change in the total perturbation energy in the system. The first term on the right side represents the vertical momentum flux transfer between the kinetic energy of the basic current and the wave energy. When shear instability occurs, the energy is transfered from the basic state shear flow to the disturbance, resulting a net loss of kinetic energy of the basic state. The second term on

the right side represents the horizontal momentum flux transfer between the kinetic energy of the basic current and the wave energy. When inertial instability occurs, the perturbation grows by extracting the kinetic energy from the horizontal basic shear. The third term on the right side represents the north-south heat flux transfer between the basic state and the perturbations. When baroclinic instability occurs, the perturbation extracts energy from the vertical shear which is supported by the northward heat flux. The fourth term represents the forcing exerted by the top boundary. It is zero if the top boundary is a flat rigid surface because that physical condition constraints w'=0 there. This term becomes negative if a radiation upper boundary condition is applied, which requires the energy generated below to propagate upward from the domain interested. The fifth term represents the forcing exerted by the lower boundary. It is zero if the lower boundary is a flat rigid boundary and positive if there exists irregular topography (e.g., a mountain). The last term on the right side of the above equation represents the energy transfer due to thermal forcing. In order for the disturbance to grow, the diabatic heating has to be added where potential temperature anomaly is positive. That is, the heat should be added in the warm region.

In this paper, we will focus on the physical characteristics of wave generation in a stably straitified fluid applicable to thermally forced mesoscale circulations in planetary atmospheres. Therefore, we will review the basic properties of inertia-gravity wave generation in the following. Those readers interested in other generation mechanisms should consult the various review papers which exist in the literature, or standard texts on the subject.

For simplicity, we consider an adiabatic linear system with constant U, N, and f. Under this situation, Eq. (2.15) reduces to

$$\left(\frac{\partial}{\partial t}+U\frac{\partial}{\partial x}\right)^2\left(\frac{\partial^2 w'}{\partial x^2}+\frac{\partial^2 w'}{\partial y^2}+\frac{\partial^2 w'}{\partial z^2}\right)+f^2\frac{\partial^2 w'}{\partial z^2}- + N^2\left(\frac{\partial^2 w'}{\partial x^2}+\frac{\partial^2 w'}{\partial y^2}\right)=0 \tag{2.20}$$

Assume a wave-like solution for w'

$$w' = \hat{w}(z)\exp[i(kx + ly - \omega t)]. \tag{2.21}$$

Substituting (2.21) into (2.20) gives

$$\frac{\partial^2 \hat{w}}{\partial z^2}+\lambda^2\hat{w}=0 , \tag{2.22}$$

where

$$\lambda^2=\frac{K^2(N^2-\Omega^2)}{\Omega^2-f^2} , \tag{2.23}$$

where K is the horizontal wave number, $(k^2+l^2)^{1/2}$, and Ω is defined to be the Doppler-shifted or intrinsic frequency, ω-kU. The solution of Eq. (2.22) can be written

$$\hat{w}\sim e^{\pm i\lambda z} . \tag{2.24}$$

Therefore, the wave property depends on the values of λ. Three different wave regimes can be identified and defined from the signs of the numerator and denominator of Eq. (2.23).

(1) $\Omega > N > f$: In this wave regime, λ is imaginary. Disturbances decay exponentially with height away from the source. Thus, the wave falls into the *evanescent wave regime*. When $\Omega >> N > f$, Eq. (2.23) reduces to

$$\lambda^2 \approx -K^2 .$$

In this extreme case, the buoyancy and rotational

forces play insignificant roles in the wave generation. The fluid behaves like a *homogeneous fluid* and the flow field may be adquately characterized as one on *potential flow*. An extensive mathematical theory exists to describe flows of this type (e.g., Lamb, 1932).

(2) $N > \Omega > f$: In this wave regime, λ is real and the wave is able to propagate freely in the vertical. Thus, the wave falls into the *vertically propagating wave regime*. One of the two possible mathematical solutions of Eq. (2.24) represents a wave propagating upward, while the other represents a wave propagating downward. For a wave generated by a low-level source such as a mountain, the Sommerfeld radiation condition requires the wave to propagate away from the energy source (i.e., upward from the mountain terrain). The other solution has no physical basis and is not retained. This also applies to the boundary condition at $z=+\infty$ for an elevated thermal forcing. However, both solutions of Eq. (2.24) must be retained in the heating layer (forcing region) and the layer between the heating base and the lower boundary (planetary surface). Since N/f typically is large in the atmosphere and the ocean, this wave regime is applicable to a wide range of intrinsic frequencies. When $N > \Omega >> f$ and $O(N) = O(\Omega)$, Eq. (2.23) reduces to

$$\lambda^2 \approx K^2 \left(\frac{N^2}{\Omega^2} - 1\right)$$

In this limit, the rotational effect may be ignored and the flow approaches the *nonhydrostatic wave regime*. When $N >> \Omega >> f$, Eq. (2.23) reduces to

$$\lambda^2 = \left(\frac{KN}{\Omega}\right)^2$$

For this case, the wave generation can be adquately determined by neglecting both the vertical acceleration and the rotational effects. Thus, the wave falls into the *nonrotating hydrostatic wave regime*. When $N >> \Omega > f$ and $O(\Omega) = O(f)$, Eq. (2.23) reduces to

$$\lambda^2 = \frac{K^2 N^2}{\Omega^2 - f^2}$$

In this limit, the vertical acceleration may be neglected in comparison with the buoyancy acceleration. Therefore, the flow approaches a hydrostatic balance and the wave falls into the *rotating hydrostatic regime*. For the case with $N > \Omega >> f$, the rotational effect can be neglected. Therefore the wave falls into the *pure gravity wave regime*.

(3) $N > f > \Omega$: In this wave regime, λ is imaginary. Similar to the first case, disturbances decay exponentially with height away from the source. Thus, the wave falls into the *evanescent wave regime*. However, the wave frequency is low. When $N > f >> \Omega$, the inertial terms, i.e. acceleration terms, play minor roles in the wave generation. The flow is characterized as being *quasi-geostrophic*. In this wave regime, the fluid motion is nearly horizontal.

From the incompressible continuity equation, it can be shown that inertia-gravity waves are transverse to the flow. That is, the fluid particle motion is perpendicular to the wave vector. In addition, the velocity vector associated with a plane inertia-gravity wave rotates anticyclonically with time. The projection of the motion on the horizontal plane is an ellipse with ω/f as the ratio of major and minor axes.

Since the wave energy propagates with the group velocity, it is important to discuss the group velocity of inertia-gravity waves. Assuming the vertical eigenfunctions to be of the form $\hat{w}(z) \sim \exp(imz)$ and substituting into Eq. (2.22) yields the dispersion

relation for inertia-gravity waves in a quiescent (motionless basic state), continuously stratified fluid.

$$\omega^2 = \frac{f^2m^2+K^2N^2}{k^2+l^2+m^2}. \tag{2.25}$$

The group velocity for inertia-gravity waves can be found by taking the derivatives of the frequency with respect to wavenumber, i.e.

$$c_{gx} = \partial\omega/\partial k, \quad c_{gy} = \partial\omega/\partial l, \quad c_{gz} = \partial\omega/\partial m. \tag{2.26}$$

Applying the above definitions to the the dispersion relation for inertia-gravity waves, Eq. (2.25), gives

$$c_{gx} = \frac{km^2(N^2-f^2)}{(k^2+l^2+m^2)^{3/2}(f^2m^2+K^2N^2)^{1/2}}, \tag{2.27a}$$

$$c_{gy} = \frac{lm^2(N^2-f^2)}{(k^2+l^2+m^2)^{3/2}(f^2m^2+K^2N^2)^{1/2}}, \tag{2.27b}$$

$$c_{gy} = \frac{-mK^2(N^2-f^2)}{(k^2+l^2+m^2)^{3/2}(f^2m^2+K^2N^2)^{1/2}}. \tag{2.27c}$$

It can be shown that

$$\mathbf{c_g} \cdot \mathbf{k} = 0, \tag{2.28}$$

where $\mathbf{k}=(k, l, m)$ is the wave vector. Thus, the group velocity vector for inertia-gravity waves is perpendicular to the wave vector.

One of the more important phenomena associated with gravity waves is wave reflection. If the basic atmospheric structure, such as the Brunt-Vaisala frequency and the basic wind speed, are allowed to vary with height, then the gravity wave may be reflected from the interface at which a rapid change of the basic atmospheric structure occurs. Consider small-amplitude perturbations in a two-dimensional nonrotating system governed by the set of Eqs. (2.22) and (2.23) but whose basic state is generalized to allow the basic wind and Brunt-Vaisala frequency to vary with height. The governing equation for $\hat{w}$ may be written as

$$\frac{\partial^2\hat{w}}{\partial z^2} + \lambda^2(z)\,\hat{w} = 0, \tag{2.29}$$

where

$$\lambda^2(z) = \frac{1}{c-U}\frac{d^2U}{dz^2} + \frac{N^2}{(c-U)^2} - k^2. \tag{2.30}$$

The above equation is a simplified version of the Taylor-Goldstein equation which was first derived independently by Taylor (1931) and Goldstein (1931). As discussed above, the solution of Eq. (2.29) is of the form $\exp(\pm i\lambda z)$. If λ^2 changes sign from positive to negative at a certain level, then λ will change from being a real to an imaginary number. This indicates a transition from the vertically propagating wave regime to the evanescent wave regime. Therefore, if a wave-like disturbance exists below that particular level, it will decay exponentially above that level. Under this situation, the wave energy is not able to propagate vertically above that particular level freely and is forced to reflect back from there. Therefore, this level is called the *wave reflection level*. If there exists such a level above the rigid (lower) surface, this atmospheric layer then acts as a waveguide trapping the wave energy between the reflection level and the surface and which allows for effective far downstream propagation of the wave energy. One well-known example of gravity wave reflection are the lee waves generated by stratified flow over a mountain range.

Another important phenomenon associated with gravity waves is the change of wave property in passing through a critical level. A critical level (z_c) is defined as the level at which the vertically sheared

basic flow U(z) is equal to the horizontal phase speed (c), i.e. $U(z_c)=c$. Using the WKB method, Bretherton (1966) showed that an upward propagating internal wave packet would approach the critical layer for the dominant frequency and wavenumber of the packet. However, it would not reach the critical layer in any finite time since along a ray path, $dz/dt \propto (z-z_c)^2$ as $z \to z_c$, which gives $t-t_0 \propto 1/(z-z_c)$ as $z \to z_c$. This means that it will take an infinite amount of time for the wave packet to reach the critical level. Thus, Bretherton inferred that the internal wave is physically absorbed at the critical level, instead of being transmitted or reflected. Mathematically, the governing equation (2.29) becomes singular at $z=z_c$. To discuss the wave properties near the critical level, we follow the study of Booker and Bretherton (1967) and the review of LeBlond and Mysak (1978). These authors used the method of Frobenius (e.g., see Hildebrand, 1976) in order to extract information about the wave behaviour near the critical level. Notice that the WKB method is not valid near the critical level since it requires a large Richardson number (N^2/U_z^2).

At $z=z_c$, U and N may be expanded in power series

$$U = c + U_{zc}(z-z_c) + \cdots$$
$$N = N_c + N_{zc}(z-z_c) + \cdots \qquad (2.31)$$

where the subscript c denotes the value at the critical level. We assume that z_c is a regular singularity which requires $U_{zc} \neq 0$. A series solution may be found near z_c (carets are dropped)

$$\begin{aligned} w(z) &\approx A(z-z_c)^{1/2+i\mu} + B(z-z_c)^{1/2-i\mu} \\ &= A \exp\left[\left(\tfrac{1}{2} + i\mu\right)\left(\ln|z-z_c| + i \arg(z-z_c)\right)\right] \\ &\quad B \exp\left[\left(\tfrac{1}{2} - i\mu\right)\left(\ln|z-z_c| + i \arg(z-z_c)\right)\right] \\ &\equiv w_A + w_B \end{aligned} \qquad (2.32)$$

Both w_A and w_B have a branch point at $z=z_c$. For the sake of definiteness we may choose that branch of the ln function for which $\arg(z-z_c)=0$ when $z>z_c$ and introduce the branch cut from $z=z_c$ along the negative x-axis. Therefore, we obtain

$$\begin{aligned} w_A^+ &= A\sqrt{|z-z_c|}\exp[i\mu \ln(z-z_c)] \\ w_B^+ &= B\sqrt{|z-z_c|}\exp[-i\mu \ln(z-z_c)] \end{aligned} \qquad \text{for } z > z_c \qquad (2.33)$$

As $z-z_c$ decreases continuously from positive to negative values, $\arg(z-z_c)$ can change continuously from 0 to π or 0 to $-\pi$. To determine the argument, we may add a small Rayleigh friction with a positive coefficient ν. The term U-c then becomes $U-c-ic_i$ where $c_i = \nu/k$. This lifts the z_c to be above the branch cut for $U_{zc}>0$, which corresponds to the contour in the lower half plane under the branch cut in an inviscid flow (Fig. 7). That is, $\arg(z-z_c)$ changes from 0 to $-\pi$ for $U_{zc}>0$. Thus, we must choose $\arg(z-z_c) = -\pi \operatorname{sgn} U_{zc}$ when $z<z_c$. Substituting this into Eq. (2.32) yields

$$\begin{aligned} w_A^- &= A\sqrt{|z-z_c|}\exp[i\mu \ln(z-z_c) - (1/2)\pi i \operatorname{sgn} U_{zc} + \mu\pi \operatorname{sgn} U_{zc}] \\ w_B^- &= B\sqrt{|z-z_c|}\exp[-i\mu \ln(z-z_c) - (1/2)\pi i \operatorname{sgn} U_{zc} - \mu\pi \operatorname{sgn} U_{zc}] \end{aligned} \qquad \text{for } z < z_c \qquad (2.34)$$

Both solutions w_A and w_B satisfy the governing equation mathematically. From Eqs. (2.33) and (2.34), we have

$$\left|\frac{w_A^+}{w_A^-}\right| = \exp(-\mu\pi \operatorname{sgn} U_{zc}), \quad \left|\frac{w_B^+}{w_B^-}\right| = \exp(\mu\pi \operatorname{sgn} U_{zc}) \qquad (2.35)$$

For $U_{zc}>0$ and a low-level forcing, the amplitude of the disturbance generated in the lower level should decrease as it crosses the critical level to the upper layer. Thus, we must choose w_A. The proper solution can be found for other situations as well. Notice that the above equation also indicates that the wave energy is attenuated exponentially through the critical level as pointed out by Booker and Bretherton

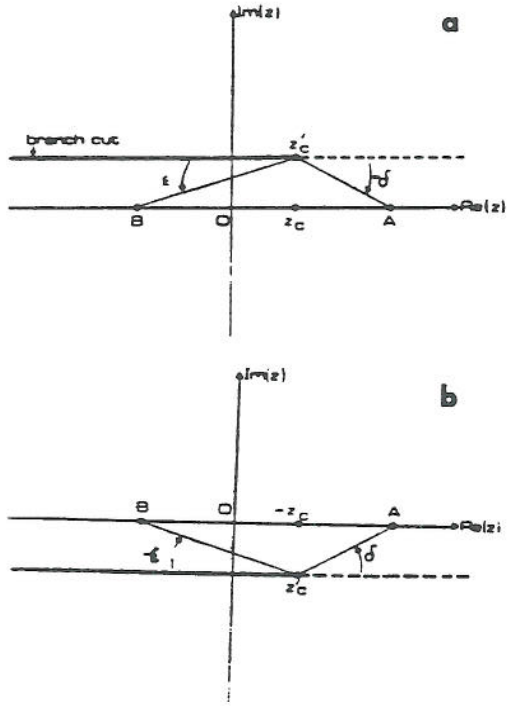

Fig. 7: Location of branch point with Rayleigh friction included for $z_c>0$, (a) $U_{zc}>0$; (b) $U_{zc}<0$. (From LeBlond and Mysak, 1978)

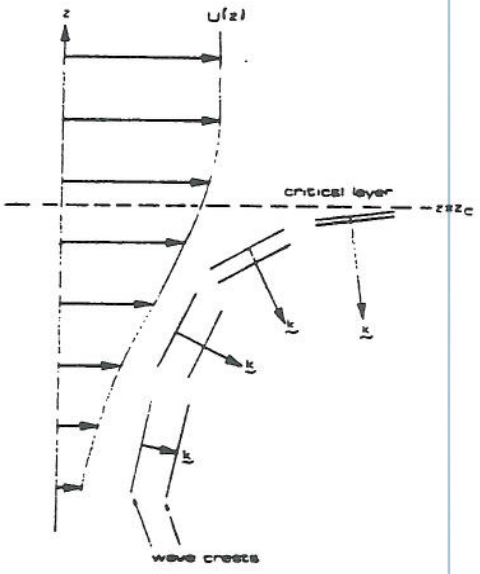

Fig. 8: The propagation of a wave packet upward toward a critical layer at $z=z_c$. The particle motions are parallel to the wave crests. Notice that the vertical wavelength becomes shorter as the wave packet approaches the critical level. (From LeBlond and Mysak, 1978, after Bretherton, 1966)

(1967). In addition, the vertical wavenumber becomes larger and the perturbation velocity becomes more and more horizontal as one approaches the critical level since

$$\lambda^2(z) \approx \frac{N^2}{(c-U)^2}. \tag{2.36}$$

This implies that $\lambda \to \infty$ as $z \to z_c$. Thus, the vertical wavelength approaches zero (Fig. 8).

3. Steady Flow over a Meso-γ Scale Heat Source

3.1 Sinusoidal heat soource

For a uniform, steady, inviscid flow over a two-dimensional meso-γ scale heat source, the Rossby number is high and the effects due to planetary rotation can be ignored. Notice that the meso-γ scale is defined to be the horizontal scale from 2 to 20 km (Orlanksi, 1975). With these assumptions, Eqs. (2.9)-(2.13) can be reduced to

$$U\frac{\partial u'}{\partial x} + \frac{1}{\rho_o}\frac{\partial p'}{\partial x} = 0 \tag{3.1}$$

$$U\frac{\partial w'}{\partial x} - g\frac{\theta'}{\theta_o} + \frac{1}{\rho_o}\frac{\partial p'}{\partial z} = 0 \tag{3.2}$$

$$\frac{\partial u'}{\partial x} + \frac{\partial w'}{\partial z} = 0 \tag{3.3}$$

$$U\frac{\partial\theta'}{\partial x}+\frac{N^2\theta_o}{g}w'=\frac{\theta_o}{c_pT_o}q' \quad . \tag{3.4}$$

The above physical system is identical to that investigated in Smith and Lin (1982) except that the perturbation potential temperature, instead of the perturbation density, is used as a dependent variable. These equations can be combined to give a single equation for the vertical velocity

$$w'_{xx}+w'_{zz}+l^2(z)\,w'=\frac{g}{c_pT_oU^2}q' \quad , \tag{3.5}$$

where $l^2(z)=N^2/U^2$ is the Scorer parameter for a uniform basic flow, which has a form of $l^2(z)=N^2/U^2-U_{zz}/U$, in general (Scorer, 1954). Similar to mountain wave theory (Smith, 1979), the above equation may be interpreted as a vorticity equation. Upon multiplying through by U, the $U(w'_{xx}+w'_{zz})$ term is the rate of change of perturbation vorticity following a fluid particle; N^2w'/U is the rate of perturbation vorticity generation by the buoyancy force; and $-U_{zz}w'$ is the rate of perturbation vorticity generation by the vertical advection of the basic vorticity (U_z).

For a quasi-steady thermal forcing, such as the surface sensible heating over a heat island, the condensational heating associated with upslope orographic rain, or the evaporative cooling under a thunderstorm, we may prescribe the heating rate q'(x,z). One simple way to obtain a mathematical solution is by assuming a separable heating function,

$$q'(x,z) = Q_o\, f(x)\, g(z) \, , \tag{3.6}$$

where g(z) is normalized according to

$$\int_0^{\infty} g(z)\, dz = 1 \quad , \tag{3.7}$$

so that

$$\rho_o\int_o^{\infty} q'(x,z)\, dz = \rho_o Q_o f(x) \tag{3.8}$$

represents the total energy in a unit time added to a vertical column of the atmosphere. To avoid the net heating problem (Smith and Lin, 1982), we impose the constraint

$$\int_{-\infty}^{\infty} f(x)\, dx = 0 \quad , \tag{3.9}$$

at each level. To find the mathematical solution, we apply a Green's function method by assuming the heating is concentrated at a height z_H,

$$q'(x,z) = Q_o\, f(x)\, \delta(z-z_H). \tag{3.10}$$

At the interface $z=z_H$, we require that the vertical velocity should be continuous, i.e.

$$w'(z_H^+) - w'(z_H^-) = 0 \quad . \tag{3.11}$$

Substituting (3.10) into (3.5) and integrating (3.5) from just below to just above $z=z_H$ gives the second interface condition,

$$w'_z(z_H^+) - w'_z(z_H^-) = \frac{g\,Q_o\,f(x)}{c_pT_oU^2} \quad . \tag{3.12}$$

Away from the interface, Eq. (3.5) reduces to Scorer's equation

$$w'_{xx}+w'_{zz}+l^2\,w'=0 \tag{3.13}$$

The mathematical problem associated with Eqs. (3.11)-(3.13) with appropriate upper and lower boundary conditions is very similar to problems encountered in mountain wave theory, which is reviewed by Queney et al. (1960) and Smith (1979).

To simplify the mathematical problem and to avoid the complications induced by the wave

reflection from the rigid, flat, lower boundary, we consider a sinusoidal heat source located at $z_H=0$, in an unbounded atmosphere.

$$q(x,z) = Q_o \cos kx\, \delta(z) \tag{3.14}$$

We look for solutions of the form

$$w'(x,z) = w_1(z) \cos kx + w_2(z) \sin kx \tag{3.15}$$

Thus, Scorer's equation which governs solutions for w_i becomes

$$w_{izz} + (l^2 - k^2)\, w_i = 0, \qquad i = 1,2 \tag{3.16}$$

To solve Eq. (3.16), we have to consider two cases: $k^2>l^2$ and $k^2<l^2$. For $k^2>l^2$, the solutions may be written as

$$w_i(x,z) = A_i(x)\, e^{-\sqrt{k^2-l^2}\,z} + B_i(x)\, e^{\sqrt{k^2-l^2}\,z}, \text{ for } z>0$$
$$w_i(x,z) = C_i(x)\, e^{-\sqrt{k^2-l^2}\,z} + D_i(x)\, e^{\sqrt{k^2-l^2}\,z}, \text{ for } z<0 \tag{3.17}$$

The B_i and C_i terms represent disturbances which grow in the vertical away from the heating level, and which should be eliminated because the energy source is located at $z_H=0$. This requires $B_i=C_i=0$. Applying the interface conditions (3.11) and (3.12) to (3.17), we obtain

$$w'(x,z) = \frac{-gQ_o}{2c_pT_oU^2\sqrt{k^2-l^2}} \cos kx\, e^{-\sqrt{k^2-l^2}\,|z|}$$
for $k^2>l^2$. (3.18)

Thus, the above solution represents evanescent waves which satisfy boundedness conditions at $z=\pm\infty$. The condition $k^2>l^2$ corresponds to $2\pi/L>N/U$ which physically represents a relatively stronger wind with a weaker stability past over a narrower heat source. The L denotes the horizontal wavelength of the heat source. Under this situation, it takes a longer time for an air parcel to undergo vertical oscillations with the Brunt-Vaisala frequency than to pass (be advected) over the heat source. In other words, the intrinsic frequency (Uk) is larger than the Brunt-Vaisala frequency. Thus, the wave energy cannot propagate away from the heat source in the vertical. Instead, it is trapped near the heating level and advected downstream. Therefore, there is no internal gravity wave generated. In the limit of $k^2>>l^2$, the buoyancy force becomes extremely weak and can be ignored. In this limiting case, the disturbance will approach a potential flow.

For the case with $k^2<l^2$, the solution of (3.16) may be written

$$w_i(z) = A_i \sin mz + B_i \cos mz, \quad i = 1,2 \tag{3.19}$$

where $m^2=l^2-k^2$. Combining with Eq. (3.15), the above solution can be rewritten as

$$w'(x,z) = C \cos(kx+mz) + D \cos(kx-mz) + E \sin(kx+mz) + F \sin(kx-mz) \quad \text{for } z>0 \tag{3.20a}$$

$$w'(x,z) = C' \cos(kx+mz) + D' \cos(kx-mz) + E' \sin(kx+mz) + F' \sin(kx-mz) \quad \text{for } z<0 \tag{3.20a}$$

Terms with argument kx+mz have an upstream phase tilt, while terms with argument kx-mz have a downstream phase tilt. Mathematically, both of them satisfy the governing equation. However, they have different physical implications. To determine the proper solution, we must calculate the vertical energy flux. Let us consider the first term

$$w'(x,z) = C \cos(kx+mz).$$

Using the continuity equation and the momentum equation, the vertical energy flux can be found

$$\int_0^L p'w'\,dx = \rho_o C^2 Um/k^2 \tag{3.21}$$

This represents an upward propagation of wave energy. Similarly, terms with argument kx-mz represent a downward propagation of wave energy. Since the energy source is located at z=0, the upper

and lower radiation conditions require D=F=C'=E'=0. Applying the interface conditions (3.11) and (3.12) to (3.20), we obtain

$$w'(x,z) = \frac{gQ_o}{2c_pT_oU^2\sqrt{l^2-k^2}} \sin\left(kx+\sqrt{l^2-k^2}\,|z|\right) \quad \text{for } k^2<l^2. \tag{3.22}$$

The above solution represents vertically propagating waves which satisfy radiation conditions at $z=\pm\infty$. The condition $k^2<l^2$ corresponds physically to a relatively weaker wind with a stronger stability over a broader heat source. Under this situation, it takes a shorter time for an air parcel to experience vertical oscillation with the Brunt-Vaisala frequency than to pass (be advected) over the heat source. In other words, the intrinsic frequency (Uk) is smaller than the Brunt-Vaisala frequency. Thus, gravity waves can be generated and the wave energy is able to propagate to positive or negative infinity (in an unbounded fluid) from the heat source. The flow response predicted by Eq. (3.22) becomes hydrostatic for $k^2<<l^2$. In this limit, the above equation reduces to

$$w' = \frac{gQ_o}{2c_pT_oU^2l} \sin(kx + l|z|) \tag{3.23}$$

Notice that the above solution repeats itself at a vertical wavelength of $2\pi U/N$. With a typical atmospheric situation of U=10 ms^{-1} and N=0.01 s^{-1}, the vertical wavelength of the forced wave is about 6.28 km.

We may define the vertical displacements as

$$w' = U\frac{\partial \eta}{\partial x} \tag{3.24}$$

The vertical displacement for the hydrostatic case is shown in Fig. 9. Vertically propagating waves are evident above and below the heating level (z=0) with phase tilting upstream. Notice that the vertical

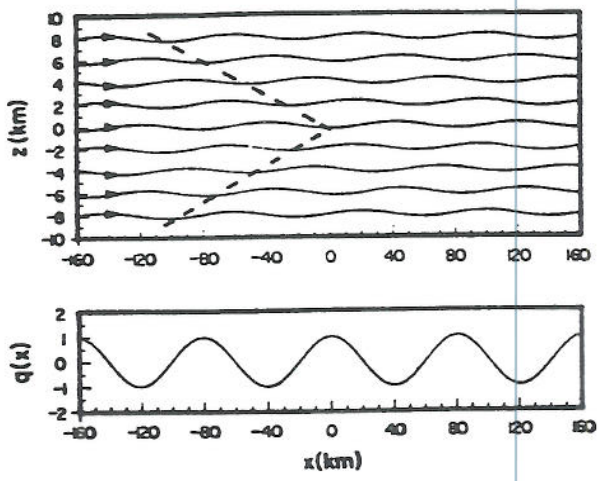

Fig. 9: The vertical displacement of an unbounded, hydrostatic, stratified airflow to perodic heating and cooling concentrated at the z=0 level, as given by Eq.(3.18) and (3.16), with U=10 ms^{-1}, N=0.01 s^{-1}, k=40 km^{-1}, Q_o=1200 W m kg^{-1}, T_o=287 K. The heating rate function is shown at the bottom of the figure. Vertically propagating waves are evident from the upstream phase tilting above and below the heating level. (From Smith and Lin, 1982)

displacement at the heating level is exactly out of phase with the heating rate. That is, the air parcel is displaced downward in the heating region, while is displaced upward in the cooling region. Smith and Lin (1982) propose a parcel argument to explain this phenomenon. This curious negative phase relationship between vertical displacement and heating will be explained later by considering the solution to the transient problem (Lin and Smith, 1986) and by using a group velocity argument (Bretherton, 1988). Proper upper and lower boundary conditions are necessary to obtain the correct solution. By using an incorrect radiation condition at infinity in an half-plane (semi-infinite

fluid) in the heat island problem, Malkus and Stern (1953) obtained a positive relationship between the heating and the vertical displacement.

Similar to applications in mountain wave theory (Eliassen and Palm, 1960), the vertical transport of horizontal momentum can be calculated by

$$MF = \rho_o \int_o^L u'w'\,dx \tag{3.25}$$

where L is the horizontal wavelength. From Eqs. (3.23) and (3.25), we obtain

$$\frac{MF}{L} = \frac{-\rho_o}{2\,kl}\left(\frac{gQ_o}{2c_pT_oU^2}\right)^2 \frac{z}{|z|} \tag{3.26}$$

The transport of mechanical energy away from the layer of forcing is accompanied by a flux of horizontal momentum towards the layer.

To examine the effect of vertical momentum flux, we may consider the time-dependent nonlinear horizontal momentum equation

$$\frac{\partial u'}{\partial t} + U\frac{\partial u'}{\partial x} + \frac{1}{\rho_o}\frac{\partial p'}{\partial x} = -u'\frac{\partial u'}{\partial x} - w'\frac{\partial u'}{\partial z} \tag{3.27}$$

Taking the horizontal integration over one wavelength yields

$$\frac{\partial \bar{u}}{\partial t} = -\frac{\partial}{\partial z}\overline{uw}, \tag{3.28}$$

where

$$\overline{(\ )} = \int_o^L (\ )\,dx \tag{3.29}$$

Therefore, convergence of the vertical momentum flux, such as that in Eq. (3.26), tends to accelerate the flow. Notice that this acceleration is not explicitly accounted for in linear theory due to the neglect of nonlinear terms. This acceleration may have relevance to the problems of wave-CISK (Raymond, 1986), heat islands, atmospheric tides, and orographic rain (Smith and Lin, 1982).

3.2 Isolated heat source and topography

The above mathematical problem is illuminative in providing physical insight of the flow response. However, in applying the theory to atmospheric phenomena, such as the orographic rain problem (Smith and Lin, 1982), we need to consider a rigid irregular lower boundary and localized heat source.

A useful localized heating function may be chosen

$$q'(x,z) = \frac{-2Q_o b^3 x}{(x^2+b^2)^2}\,\delta(z-z_H) \tag{3.30}$$

The above heating function is shown in Fig. 10 as curve 1. This heating function can be used to simulate the condensational heating and evaporative cooling associated with a nonprecipitating orographic cloud. Again, we may apply a Green's function method to obtain the solution. The heating is

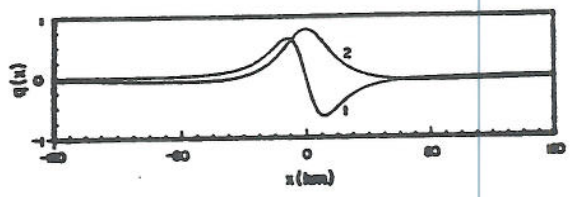

Fig. 10: The horizontal heating functions of Eq. (3.30) with b=20 km (curve 1) and Eq. (3.50) with b_1=20 and b_2=100 km (curve 2). The balanced heating and cooling function (curve 1) is used to simulate the condensational heating and evaporative cooling associated with a nonprecipitating orographic cloud. Curve 2 is used to simulate the condensational heating associated with orographic rain, with isolated heating and widespread cooling. (From Smith and Lin, 1982)

concentrated at a certain level. Substituting the above equation into Eq. (3.13), we have

$$w'_{xx} + w'_{zz} + l^2 w' = \frac{-2gQ_o b^3 x}{c_p T_o U^2 (x^2+b^2)^2} \delta(z-z_H) \tag{3.31}$$

Let $\tilde{w}(k,z)$ be the one-sided Fourier transform of $w'(x,z)$ in x, i.e.,

$$\tilde{w}(k,z) = \frac{1}{2\pi} \int_{-\infty}^{\infty} w'(x,z)\, e^{-ikx}\, dx \tag{3.32a}$$

$$w'(x,z) = 2\,\mathrm{Re} \int_0^{\infty} \tilde{w}(k,z)\, e^{ikx}\, dk \tag{3.32b}$$

Now taking the Fourier transform of Eq. (3.31), we obtain

$$\tilde{w}_{zz} + (l^2-k^2)\,\tilde{w} = \frac{igQ_o b^2 k}{c_p T_o U^2} e^{-kb} \delta(z-z_H) \tag{3.33}$$

For $z \neq z_H$, (3.33) becomes Scorer's equation (Scorer, 1954)

$$\tilde{w}_{zz} + (l^2-k^2)\,\tilde{w} = 0 \tag{3.34}$$

For a hydrostatic wave ($k^2 \ll l^2$), the solution may be written as

$$\tilde{w}(k,z) = A e^{ilz} + B e^{-ilz} \quad \text{for } 0 \le z < z_H \tag{3.35a}$$

$$\tilde{w}(k,z) = C e^{ilz} + D e^{-ilz} \quad \text{for } z_H \le z \tag{3.35b}$$

At the gound, the flow is assumed to follow the terrain, thus

$$\frac{w}{u} = \frac{w'}{U+u'} = \frac{dh(x)}{dx}, \qquad \text{at } z=h(x), \tag{3.36}$$

where h(x) represents the terrrain height. For small amplitude topography and induced disturbance, the above lower boundary condition may be written as

$$w' = U \frac{dh(x)}{dx}, \qquad \text{at } z=0. \tag{3.37}$$

For mathematical simplicity, we consider a bell-shaped function to represent the topography which is often used in mountain wave theory (e.g., Smith, 1979)

$$h(x) = \frac{h_o a^2}{(x^2+a^2)}. \tag{3.38}$$

Substituting (3.38) into (3.37) and taking the Fourier transform, we obtain

$$\tilde{w}(k,0) = ikUh_o a e^{-ka}. \tag{3.39}$$

Applying the lower boundary condition (3.39) to (3.35a) gives

$$A + B = ikUh_o a e^{-ka}. \tag{3.40}$$

The upper radiation boundary condition should allow the wave energy to propagate upward (Eliassen and Palm, 1960; Bretherton, 1969). This can be determined by computing the vertical energy flux similar to Eq. (3.21), which requires D=0. With (3.40) and this upper boundary condition, (3.35) becomes

$$\tilde{w}(k,z) = 2iA \sin lz + ik\, Uh_o a e^{-ka} e^{-ilz}, \quad \text{for } 0 \le z < z_H \tag{3.41a}$$

$$\tilde{w}(k,z) = C e^{ilz}, \quad \text{for } z \ge z_H \tag{3.41b}$$

In the above solution, we allow the thermally forced wave to propagate downward toward the surface below the heating level z_H. Coefficients A and C in (3.41) can be determinted by the two interface conditions (3.11) and (3.12). In the Fourier space, they have the following forms

$$\tilde{w}(z_H^+) - \tilde{w}(z_H^-) = 0, \tag{3.42a}$$

$$\tilde{w}_z(z_H^+) - \tilde{w}_z(z_H^-) = \frac{ig\,Q_o\,b^2 k e^{-bk}}{c_p T_o U^2}. \tag{3.42b}$$

Applying the above equation to (3.41) and taking the inverse Fourer transform lead to

$$w'(x,z) = 2\mathrm{Re}\left\{ \int_0^{\infty} \left[iUh_o ake^{-ka}e^{ilz} - \frac{igQ_o b^2 k e^{-kb} e^{ilz_H} \sin lz}{c_p T_o U^2 l} \right] e^{ikx} dk \right\}$$

for $0 \le z < z_H$

$$w'(x,z) = 2\mathrm{Re}\left\{ \int_0^{\infty} \left[iUh_o ake^{-ka}e^{ilz} - \frac{igQ_o b^2 k e^{-kb} e^{ilz} \sin lz_H}{c_p T_o U^2 l} \right] e^{ikx} dk \right\}$$

for $z \ge z_H$. (3.43)

Using the relationship (3.24), the vertical displacement be obtained

$$\eta(x,z) = \eta_m(x,z) - \frac{gQ_o b^2 \sin lz\,(b \cos lz_H - x \sin lz_H)}{c_p T_o U^3 l\,(x^2+b^2)}$$

for $0 \le z < z_H$ (3.44a)

$$\eta(x,z) = \eta_m(x,z) - \frac{gQ_o b^2 \sin lz_H\,(b \cos lz - x \sin lz)}{c_p T_o U^3 l\,(x^2+b^2)},$$

for $z \ge z_H$, (3.44b)

where

$$\eta_m(x,z) = \frac{h_o a(a\cos lz - x \sin lz)}{x^2+a^2}. \tag{3.44c}$$

Notice that the above solution is a superposition of the hydrostatic mountain wave (η_m) and the thermally forced gravity wave.

The pressure perturbation at the surface can be computed from (3.44) using either Bernoulli's equation (substituting Eqs. (3.3) and (3.24) into Eq. (3.1))

$$p'(x,0) = -\rho_o U u'(x,0) = \rho_o U^2 \frac{\partial \eta}{\partial z}\Big|_{z=0} \tag{3.45}$$

or the hydrostatic equation (with Eq.(3.4))

$$p'(x,0) = \frac{g\rho_o}{\theta_o}\int_0^{\infty} \theta'\, dz$$

$$= -\rho_o N^2 \int_0^{\infty} \eta(x,z)\, dz - \frac{g\rho_o Q_o}{c_p T_o U}\int_{-\infty}^{x} f(x)\, dx \tag{3.46}$$

Either approach gives

$$p'(x,0) = -\rho_o N U h_o \frac{ax}{x^2+a^2} - \frac{\rho_o g Q_o b^2}{c_p T_o U^2} \left\{ \frac{(b \cos lz_H - x \sin lz_H)}{(x^2+b^2)} \right\} \tag{3.47}$$

The first terms (η_m) of Eqs. (3.44) and (3.47) represent the vertical displacement and surface pressure perturbation produced by the mountain wave, which have been found by Queney (1947) and studied extensively in the literature (e.g., see Smith, 1979 for a review). The second terms of Eqs. (3.44) and (3.47) represent the vertical displacement and surface pressure disturbance produced by the thermally induced gravity wave, which satisfy the rigid lower boundary condition w'=0 at z=0, and thus the downgoing wave produced by the elevated heating is totally reflected. The vertical momentum flux is zero between the heating level and the surface, due to the flux cancellation of the up and downgoing waves. This gives no vertical phase tilt of the disturbance. The flow response is sensitive to the heating level since the upgoing and downgoing wave may cancel each other. If the heating is added very near the surface, $lz_H \ll 1$, the disturbance is extremely small and may be neglected. From Eq.

(3.44), cancellation of the direct upgoing wave and the reflected upgoing wave above z_H, can also occur at

$$lz_H = 0, \pi, 2\pi, ..., n\pi.$$

This effect is less evident if the heating is spread over a layer of finite depth.

For a heat source distributed uniformly in a layer of $z=z_H-d$ to z_H+d, the solution can be obtained by superposition of heating terms of (3.44a and b) (last terms). In order to keep the same heating rate, the amplitude of this vertically distributed heating should be reduced to $Q_o/2d$. If we write (3.44a) and (3.44b) as $\eta = \eta_m+\eta_H^-$ and $\eta = \eta_m+\eta_H^+$, respectively, then the superposition of heating terms leads to

$$\eta(x,z) = \eta_m(x,z) + \int_{z_H-d}^{z_H+d} \eta_H^-(x,z,z')\, dz' \quad \text{for } 0 \le z < z_H-d, \tag{3.48a}$$

$$\eta(x,z) = \eta_m(x,z) + \int_{z_H-d}^{z} \eta_H^+(x,z,z')\, dz' + \int_{z}^{z_H+d} \eta_H^-(x,z,z')\, dz' \quad \text{for } z_H-d \le z < z_H+d, \tag{3.48b}$$

$$\eta(x,z) = \eta_m(x,z) + \int_{z_H-d}^{z_H+d} \eta_H^+(x,z,z')\, dz' \quad \text{for } z_H+d \le z, \tag{3.48c}$$

where z' represents z_H in (3.44) and acts as an integral variable in the above equation. The final solution can be obtained

$$\eta(x,z) = \eta_m(x,z) - \frac{gQ_ob^2\sin lz}{c_pT_oU^3l^2(x^2+b^2)}[b\{\sin l(z_H+d) - \sin l(z_H-d)\}+x\{\cos l(z_H+d)-\cos l(z_H-d)\}] \quad \text{for } 0 \le z < z_H-d \tag{3.49a}$$

$$\eta(x,z)=\eta_m(x,z)+\frac{gQ_ob^2}{c_pT_oU^3l^2(x^2+b^2)}\{(b\cos lz - x\sin lz)\{\cos lz-\cos l(z_H-d)\} - \sin lz\,[b\{\sin l(z_H+d)-\sin lz\} +x\{\cos l(z_H+d)-\cos lz\}]\} \quad \text{for } z_H-d \le z < z_H+d \tag{3.49b}$$

$$\eta(x,z)=\eta_m(x,z)+\frac{gQ_ob^2}{c_pT_oU^3l^2(x^2+b^2)}(b\cos lz - x\sin lz)\cdot\{\cos l(z_H+d)-\cos l(z_H-d)\} \quad \text{for } z_H+d \le z. \tag{3.49c}$$

Another useful heating function is

$$q'(x,z) = Q_o\left(\frac{b_1^2}{x^2+b_1^2} - \frac{b_1b_2}{x^2+b_2^2}\right)\delta(z-z_H), \tag{3.50}$$

where b_1 and b_2 are the half-width of the isolated heating and the widespread compensated cooling, respectively. The widespread cooling is used to avoid the net heating problem (Smith and Lin, 1982). This problem will be discussed in Section 4. The above function may be used to simulate the condensational heating associated with a precipitating orographic cloud. Applying the method used above, the following solutions may be derived

$$\eta(x,z) = \eta_m(x,z) - \frac{gQ_ob_1\sin lz}{c_pT_oU^3l}\left\{(\cos lz_H)\left(\tan^{-1}\frac{x}{b_1} - \tan^{-1}\frac{x}{b_2}\right) + \frac{1}{2}(\sin lz_H)\ln\left(\frac{x^2+b_2^2}{x^2+b_1^2}\right)\right\} \quad \text{for } 0 \le z < z_H \tag{3.51a}$$

$$\eta(x,z) = \eta_m(x,z) - \frac{gQ_ob_1\sin lz_H}{c_pT_oU^3l}\left\{(\cos lz)\left(\tan^{-1}\frac{x}{b_1} - \tan^{-1}\frac{x}{b_2}\right) + \frac{1}{2}(\sin lz)\ln\left(\frac{x^2+b_2^2}{x^2+b_1^2}\right)\right\} \quad \text{for } z_H \le z \tag{3.51b}$$

The perturbation surface pressure associated with (3.51) is

$$p'(x,0) = -\rho_oNUh_o\frac{ax}{x^2+a^2} - \frac{\rho_ogQ_ob_1}{c_pT_oU}\left\{(\cos(lz_H)\right.$$

$$\left(\tan^{-1}\frac{x}{b_1} - \tan^{-1}\frac{x}{b_2}\right) + \frac{1}{2}(\cos(lz_H)\ln\left(\frac{x^2+b_2^2}{x^2+b_1^2}\right)\Bigg\} \tag{3.52}$$

If this isolated heat source is distributed uniformly in a layer from $z=z_H-d$ to z_H+d, the method of superposition discussed above may be used to obtain the result

$$\eta(x,z) = \eta_m(x,z) - \frac{gQ_0b_1\sin lz}{c_pT_oU^3l^2}\left\{\left(\tan^{-1}\frac{x}{b_1} - \tan^{-1}\frac{x}{b_2}\right)\cdot[\sin l(z_H+d)-\sin l(z_H-d)] - \frac{1}{2}\ln\left(\frac{x^2+b_2^2}{x^2+b_1^2}\right)\cdot[\cos l(z_H+d)-\cos l(z_H-d)]\right\}$$
$$\text{for } 0 \le z < z_H \tag{3.53a}$$

$$\eta(x,z) = \eta_m(x,z) + \frac{gQ_0b_1}{c_pT_oU^3l^2}\left\{(\cos lz)\left(\tan^{-1}\frac{x}{b_1} - \tan^{-1}\frac{x}{b_2}\right) + \frac{1}{2}(\sin lz)\ln\left(\frac{x^2+b_2^2}{x^2+b_1^2}\right)\cdot[\cos lz - \cos l(z_H-d)]\right\} - \frac{gQ_0b_1\sin lz}{c_pT_oU^3l^2}\left\{\left(\tan^{-1}\frac{x}{b_1} - \tan^{-1}\frac{x}{b_2}\right)\cdot[\sin l(z_H+d)-\sin lz] - \frac{1}{2}\ln\left(\frac{x^2+b_2^2}{x^2+b_1^2}\right)\cdot[\cos l(z_H+d)-\cos lz]\right\}$$
$$\text{for } z_H-d \le z < z_H+d \tag{3.53b}$$

$$\eta(x,z) = \eta_m(x,z) + \frac{gQ_0b_1}{c_pT_oU^3l^2}\left\{(\cos lz)\left(\tan^{-1}\frac{x}{b_1} - \tan^{-1}\frac{x}{b_2}\right) + \frac{1}{2}(\sin lz)\ln\left(\frac{x^2+b_2^2}{x^2+b_1^2}\right)\right\}\cdot[\cos l(z_H+d)-\cos l(z_H-d)]$$
$$\text{for } z_H+d \le z \tag{3.53c}$$

The hydrostatic response of a balanced heating and cooling (Eq. (3.30)) added at $z_H=\pi/2l\approx1.57$ km is given in Fig. 11. The solution is given by the second terms of (3.44) with $Q_0=1107$ Wmkg^{-1}, b=20 km, U=10 ms^{-1}, and N=0.01 s^{-1}. The upstream phase tilt of the thermally forced gravity waves is evident above the heating level. Notice that a downward displacement is produced near the heating region and upward displacement near the cooling region. The result of Malkus and Stern (1953) would be similar to the present one if they used the correct upper radiation condition. This relationship will be explained in the next section. The vertical displacement at the heating level is repeated every 6.28 km ($2\pi/l$). The surface perturbation pressure is shown at the lower panel of Fig. 11. The hydrostatic equation indicates that the surface pressure is an integral measure of the temperature or density anomaly aloft. Eq. (3.46) or the thermodynamic equation implies that the

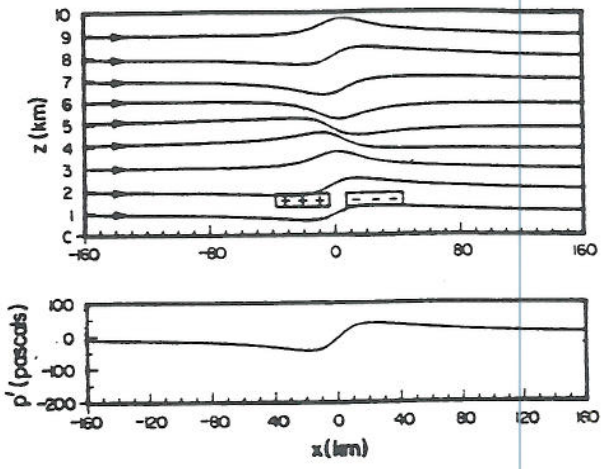

Fig. 11: The vertical displacement of a hydrostatic airflow to balanced heating and cooling (Eq.(3.30)) concentrated at $z_H=1.57$ km in an half plane. Regions with large heating and cooling are marked +++ and - - -, respectively. This flow is given by the second terms of Eq. (3.44) with $Q_0=1107$ W m kg^{-1}, b=20 km, U=10 ms^{-1}, and N=0.01 s^{-1}. Vertically propagating waves are present above the heating level. The surface pressure disturbance (in Pa) is shown in the lower panel. (From Smith and Lin, 1982)

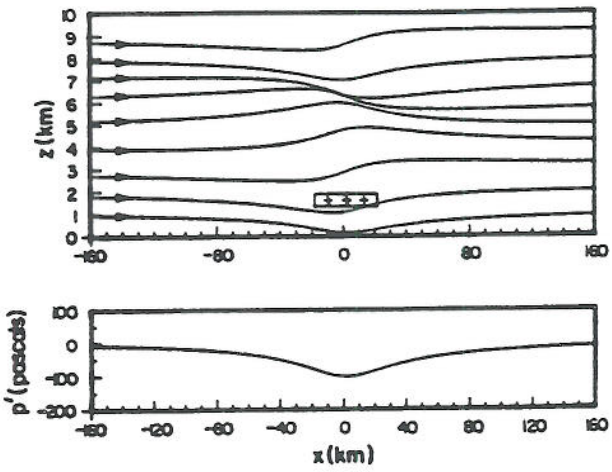

Fig. 12: Same as Fig. 11 except for the isolated heating-widespread cooling function (3.50). The solution is given by the second terms of Eq.(3.51) with Q_0=900 W m kg^{-1}, b_1=20 km, b_2=100 km, U=10 m s^{-1}, N=0.01 s^{-1}. The perturbation surface pressure is shown in the lower panel, which is negative directly below the region of heating. (From Smith and Lin, 1982)

temperature anomaly may be caused directly by the heating and indirectly from the thermally-induced vertical motion. According to Bernoullis' equation, the wind speed is increased when the streamlines are closer together. One example of the response of a hydrostatic airflow over this isolated heating and compensated cooling (Eq.(3.50) is shown in Fig. 12. The heating is added at $z_H=\pi/2l$. The solution is given by Eq.(3.51) with η_m ignored and Q_0=900 W m kg^{-1}, b_1=20 km, b_2=100 km, U=10 ms^{-1}, and N=0.01 s^{-1}. The response is similar to the previous case. The relationship between the thermal response in a system with and without a basic flow is discussed by Thorpe et al. (1980). The large Froude number results in that paper are in qualitative agreement with the present results. Hsu (1987a,b) found a similar result for a mesoscale flow over a finite surface heating. The heating in that paper is added into the system through conduction by prescribing the perturbation surface potential temperature.

3.3 Applications

The theory developed in Section 3.2 has been applied to the problem of orographic rain by Smith and Lin (1982, 1983). Based on the formation mechanisms, the orographic rain may be classified as follows:

(1) Upslope orographic rain in a stable atmosphere (Sarker, 1967)

(2) Orographic rain in a conditionally unstable atmosphere (Davies and Schar, 1986)

  (a) uplsope rain, instability released by forced orographic ascent.

    (i) shallow convection embedded within frontal clouds in midlatitude (Browning et al., 1974; 1980; Hobbs et al., 1975; Marwitz, 1980)

    (ii) closely packed deep convection in tropics (Smith and Lin,1983).

  (b) lee convective rain, instability triggered by slope heating (Henz, 1972).

(3) Orographic rain over small hills by seeder cloud-feeder cloud mechanism (Bergeron, 1968; Browning, 1980).

(4) Existing baroclinicity which, through the action of orographic blocking and differential advection, can lead to an unstable air column (Smith, 1982).

For a quasi-steady nonprecipitating orographic cloud, the condensational heating and evaporative cooling may be represented by the balanced heating and cooling (Eq.(3.30)). An example of a hydrostatic airflow over a bell-shaped mountain with and without diabatic heating is given in Fig. 13. The disturbance induced by combined mechanical and

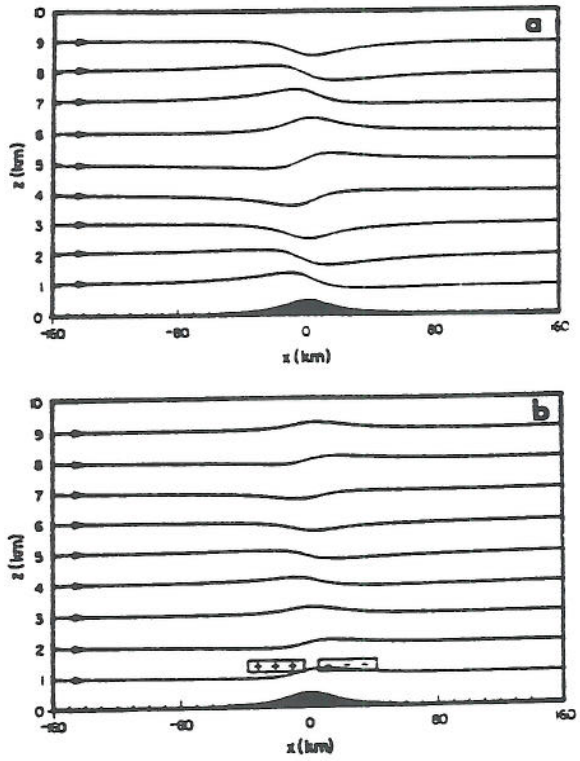

Fig. 13: (a) The vertical displacement of a hydrostatic adiabatic flow over a bell-shaped mountain. The solution is first derived by Queney (1947) and given by Eq.(3.44c) with h_o=500 m, a=20 km, U=10 m s^{-1}, and N=0.01 s^{-1}. (b) Hydrostatic flow over a combined thermal and orographic forcing. The prescribed diabatic heating represents a nonprecipitating orographic cloud. The solution is given by Eq.(3.44a and b) with Q_o=1107 W m kg^{-1}, b=20 km, U=10 ms^{-1}, and N=0.01 s^{-1}. The induced disturbance is weaker than the adiabatic mountain wave (a). (From Smith and Lin, 1982)

thermal forcing is weaker than the adiabatic flow (Fig. 13a). The vertical displacement near the heating region is consistent with previous results. That is, heating (cooling) produces downward (upward) displacement. The relative magnitude of the response can be found from the ratio of the two coefficients in Eq.(3.44),

$$\frac{gQ_o b}{c_p T_o U^2 N h_o}$$

where Q_o and b are roughly related to the intensity and the horizontal scale of the observed rainfall at the

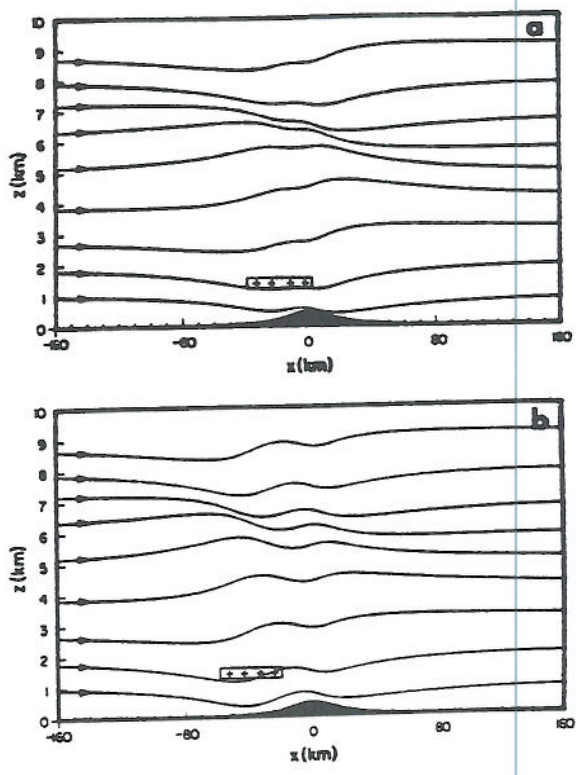

Fig. 14: The vertical displacement of a hydrostatic flow over combined thermal and orographic forcing. The diabatic heating represents an upslope precipitating orographic rain. The solution is given by Eq.(3.51) with x replaced by x+c and Q_o=900 W m kg^{-1}, b_1=20 km, b_2=100 km, U=10 m s^{-1}, and N=0.01 s^{-1}. The upstream displacement of heating of c=20 km is shown in (a) and c=40 km in (b). (From Smith and Lin, 1982)

surface. Fig. 14 shows two examples of hydrostatic responses in a stratified airflow to isolated thermal and orographic forcing. The solution is given by Eq.(3.51) with x in the second terms of Eq.(3.51) replaced by x+c, where c is the upstream distance between the heating center and the mountain top. Notice the significant difference in the flow patterns due to the different upstream displacements of the thermal forcing.

The significance of the combined thermal and orographic forcing can be seen from the vertical transport of horizontal momentum. The momentum flux corresponding to Eq.(3.51) with x replaced by x+c is

$$MF = -\frac{\pi}{4}\rho_o h_o^2 NU - \left(\frac{\pi a g \rho_o h_o Q_o b_1}{c_p T_o U}\right) \left[\frac{(a+b_1)\cos lz_H - c \sin lz_H}{(a+b_1)^2+c^2} - \frac{(a+b_2)\cos lz_H - c \sin lz_H}{(a+b_2)^2+c^2}\right] \quad \text{for } 0 \le z < z_H \qquad (3.54a)$$

$$MF = -\frac{\pi}{4}\rho_o h_o^2 NU - \frac{\pi \rho_o}{l}\left(\frac{g Q_o b_1 \sin lz_H}{c_p T_o U^2}\right)^2 \cdot \ln\left[\frac{(b_1+b_2)^2}{4b_1 b_2}\right] + \left(\frac{\pi a g \rho_o h_o Q_o b_1 \sin lz_H}{c_p T_o U}\right) \cdot \left[\frac{2c}{(a+b_1)^2+c^2} - \frac{2c}{(a+b_2)^2+c^2}\right] \quad \text{for } z_H \le z \qquad (3.54b)$$

The first terms in the above equation result from the vertically propagating mountain waves, which are negatively proportional to the vertical energy flux which is constant with height for an adiabatic flow with no critical level and diabatic heating (Eliassen and Palm, 1960). Note that besides the pure h^2 and Q_o^2 terms there are cross terms proportional to $h_o Q_o$. The existence of this important contribution to the momentum flux below the heating level (Eq.(3.54a)) can be explained as arising physically from the thermally generated pressure disturbance at the surface, acting on the topography. It could therefore be computed directly from the perturbation surface pressure (Eq.(3.52)) together with (3.38). If a large amount of heating occurs over the windward slope of a mountain, the pressure at the surface could be lowered sufficiently to cause a reversal of the expected downstream drag. The vertical profiles of momentum flux corresponding to the adiabatic mountain wave (Fig. 13a) and the thermally and orographically forced wave (Fig. 14a) are shown in Fig. 15. In Eq.(3.54), the cross terms of the momentum flux depend on the relative horizontal position of the heating and the mountain, i.e., c. As mentioned earlier, the pure thermally induced flux (Q_o^2) term must vanish below the heating level because of wave reflection from the surface.

A good example of the local enhancement of precipitation by orography is the large annual rainfall

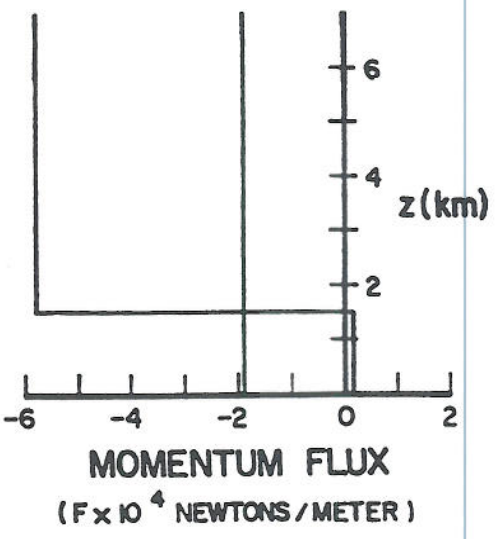

Fig. 15: The vertical profile of momentum flux for the cases shown in Figs. 13a and 14a as given by Eq.(3.54). In an adiabatic flow the flux is constant with height. In the presence of thermal forcing, the mountain drag is reversed and the momentum flux is strongly convergent at the heating level. (From Smith and Lin, 1982)

recorded along the Malabar Coast and on the windward slopes of the Western Ghats in India (Fig. 16). This rainfall occurs almost entirely during the 3-4 month summer period when the coast lies in the path of the west-southwest monsoon current crossing the Arabian Sea (Fig. 17). The low-level wind has a speed of about 15 ms^{-1} (at 850 mb), and a direction more or less perpendicular to the coast. In the upper troposphere, the wind is reversed, blowing from the east as part of the subtropical easterly. Fig. 18 shows a hydrostatic flow with combined thermal and orographic forcing (Smith and Lin, 1983). The heating is producing a disturbance which is at least as large as that of the mountain. As

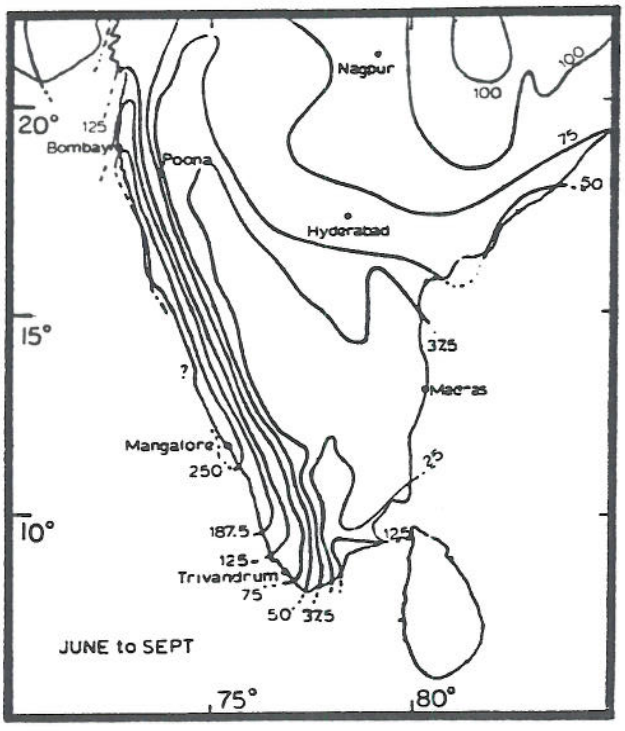

Fig. 16: The areal distribution of rainfall over India during the summer monsoon months of June to September (from Smith and Lin, 1983, after Ramakrishan and Rao, 1958). The rainfall is concentrated just upstream of the Western Ghats.

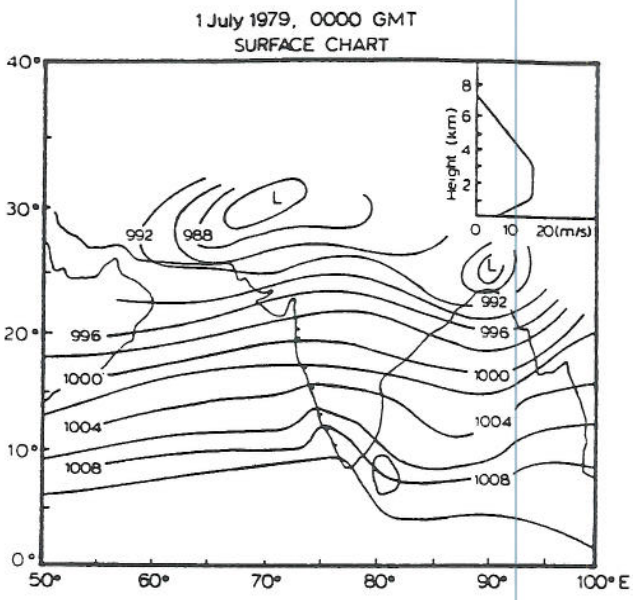

Fig. 17: A typical surface chart for the Indian Ocean during the summer monsoon. This particular chart is for 1 July 1979 at 0000 GMT. The horizontal wind perpendicular to the coast is shown at the upper right corner. (From Smith and Lin, 1983)

mentioned earlier (Eq. (3.44)), the thermally-induced disturbance is moderately sensitive to the choice of lz_H. For the present choice of z_H=3km, there is a region of strong low-level convergence and ascent which may be able to trigger cumulus growth. This choice is reasonable as waves generated in the upper troposphere would be absorbed by the critical level in midtroposphere (Fig. 17). Fig. 18 also indicates that there is a wide pressure trough produced by the heating, which is absent in the adiabatic case. The pressure trough may be related to the offshore trough often observed during the rainy spell of the monsoon period.

Using the data from WMO/ICSU Summer Monsoon Experiment and a two-dimensional

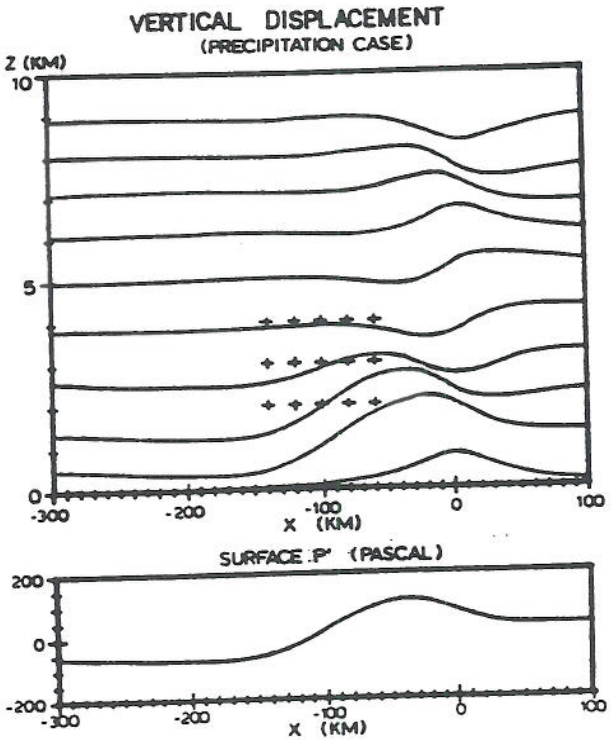

Fig. 18: The vertical displacement of a hydrostatic flow with thermal and orographic forcing. Region of the isolated heating is denoted by "+++". The solution is given by Eq. (3.53) with Q_0=1200 W m^{-2}, b_1=40 km, b_2=200 km, a=40 km, h_0=800 m, z_H=3 km, d=1.5 km, U=10 ms^{-1}, N=0.01 s^{-1}. The heating center is displaced upstream by 100 km (c). The surface perturbation pressure is drawn at the bottom. Note that there is a wide pressure trough produced by the heating. (From Smith and Lin, 1983)

nonlinear model, Grossman and Durran (1984) have shown that the Western Ghats produce a deceleration and convergence of the southwest monsoon winds, triggering deep convection over the Arabian Sea. The results seem consistent with results of Smith and Lin (1983). However, as commented on by Smith (1985), the effect of latent heating has been omitted in that study. Using a two-dimensional compressible moist cloud model to simulate flow over the Western Ghats, Ogura and Yoshizaki (1988) find that in order to account for the observed features of rainfall over the Arabian Sea and the Ghat Mountains during the summer monsoon season, the strongly sheared environment and fluxes of latent and sensible heat from the ocean are essential. It appears that a theory which includes these factors can be constructed, similar to that of Lin (1987), and compared with the numerical results of Ogura and Yoshizaki. The combined effect of thermal and orographic forcing has also been studied by Davies and Schar (1986). In their theory, they incorporated a CISK-like representation for non-precipitating convective cloud in a linear, steady, hydrostatic flow over a mountain ridge. They found that the combined effect of the two forcing processes can be significantly different from that of orography acting alone. In particular, in certain situations an enhanced (resonant) response can occur with strong winds on the lee slope and a concomitant large surface pressure drag. Their results help to clarify the disparate results obtained in earlier studies, and, unlike those studies, suggest that diabatic effects might on occasions have a major role in inducing strong surface lee-side winds.

Similar theories have also been developed and applied to the mesoscale lake-effects on the generation of snowstorms in the vicinity of Michigan Lake (Hsu, 1987a, b) and the steady state response of the atmosphere to prescribed temperature perturbations corresponding to melting snow (Lin, C.A. et al., 1988a,b; Robichaud and Lin, C.A., 1989).

4. Transient Flow over a Meso-γ Scale Heat Source

Mesoscale problems of thermal or mechanical

forcing cannot be fully understood using a steady state model. The importance of solving a time-dependent problem has been demonstrated in the studies of mountain waves (e.g., Hoiland, 1951; Palm, 1953; Queney, 1954), which provided insight into how a forced perturbation is established when the wind becomes practically steady over mountainous terrain. The transient heat island problem has been treated by Smith (1957), but without a full discussion of the energetics and the problematic approach to steady state. The internal gravity waves generated by local prescribed heating have been investigated by Blumen and Hendl (1969) with application to Joule heating in the ionsphere. The mathematical problem of wave generation by local thermal sources also arises in the study of large explosions (e.g., Pekeris, 1948; Scoror, 1950; Hunt et al., 1960; Weston, 1962). These studies, however, are primarily concerned with the far field radiation of acoustic-gravity waves. In this section, we will review the transient response of a flow to a meso-γ scale heat source investigated by Lin and Smith (1986).

4.1 Flow response to a pulse heating

Consider a two-dimensional, inviscid, nonrotating, hydrostatic, Boussinesq flow. The governing equation can be reduced from Eq. (2.15) or extended from Eq. (3.5) to be

$$\left(\frac{\partial}{\partial t} + U\frac{\partial}{\partial x}\right)^2 w'_{zz} + N^2 w'_{xx} = \frac{g}{c_p T_o} q'_{xx} \quad (4.1)$$

To solve the above equation, we again apply the Green's function method in the vertical direction. Taking the Fourier transform in x (x -->k) and Laplace transform in t (t -->s) of the above equation, we have

$$\hat{w}_{zz} + \lambda^2 \hat{w} = \frac{g\lambda^2}{c_p T_o N^2} \hat{q}, \quad (4.2)$$

where

$$\lambda \equiv \frac{iNk}{s + iUk}, \quad \text{and } \mathrm{Re}(s) > 0.$$

Assume the heating is released in a very short time period as a pulse at a single level, z=0, in an unbounded fluid,

$$q'(t,x,z) = Q_o \left(\frac{b^2}{x^2 + b^2}\right) \delta(z)\, \delta(t). \quad (4.3)$$

Taking the Fourier and Laplace transforms of the above equation and substituting into Eq. (4.2) gives

$$\hat{w}_{zz} + \lambda^2 \hat{w} = \frac{gQ_o b\lambda^2 e^{-bk}}{c_p T_o N^2} \delta(z). \quad (4.4)$$

Similar to the steady state problem, the interface condition can be obtained by assuming the continuity of the vertical velocity at the interface (z=0) and integrating the above equation across it. That is,

$$\hat{w}(0^+) - \hat{w}(0^-) = 0, \quad (4.5)$$

$$\hat{w}_z(0^+) - \hat{w}_z(0^-) = \frac{gQ_o b\lambda^2 e^{-bk}}{c_p T_o N^2}. \quad (4.6)$$

An appropriate set of upper and lower boundary conditions for an unbounded fluid are the Sommerfeld radiation conditions, i.e.

$$\hat{w} \sim e^{i\lambda|z|} \quad \text{as } |z| \to \infty \quad (4.7)$$

Thus, the solution of Eq. (4.4) can be obtained

$$\hat{w}(s, k, z) = \frac{-igQ_o b}{2c_p T_o N^2} \lambda e^{-bk} e^{i\lambda|z|}. \quad (4.8)$$

The above solution decays at infinity because Re(s)>0. The vertical displacement, η, defined by

$$w' = \frac{D\eta}{Dt} = \frac{\partial \eta}{\partial t} + U\frac{\partial \eta}{\partial x}, \tag{4.9}$$

may be written as

$$\hat{\eta}(s, k, z) = \frac{gQ_o bke^{-bk}}{2c_pT_oN(s+iUk)^2} \exp\left(-\frac{Nk|z|}{s+iUk}\right). \tag{4.10}$$

The inverse Lapalce transform of the above equation can be performed to obtain

$$\tilde{\eta}(t, k, z) = \frac{gQ_o bke^{-bk}}{2c_pT_o} \left(\frac{t}{Nk|z|}\right)^{1/2} e^{-iUkt}\ J_1(2\sqrt{Nk|z|t}), \tag{4.11}$$

where $\tilde{\eta}$ denotes the Fourier transform of η and J_1 the Bessel function of order 1. The inverse Fourier transform can also be performed to yield the solution in physical space

$$\eta(t, x, z) = \frac{gbQ_o t}{2c_pT_oN(X^2+b^2)^2} \exp\left(\frac{-Nb|z|}{X^2+b^2}\right) \cdot \left[(b^2-X^2)\cos\left(\frac{NX|z|}{X^2+b^2}\right) + 2bX \sin\left(\frac{NX|z|}{X^2+b^2}\right)\right], \tag{4.12}$$

where X=x-Ut is the horizontal coordinate in the reference frame moving with the basic wind. In the moving frame, the above equation is just the response of the fluid to a pulse heating in a quiescient stratified fluid.

The solution for a more realistic heating function in the vertical can be obtained by use of Green's function method. The rigid lower boundary can also be incorporated by applying the method of images. The vertical displacement for a pulse heating distributed uniformly in a layer from z_o-d to z_o+d in a half plane can be written as

$$\eta(t, x, z) = \frac{A}{(X^2+b^2)} \Big\{ 2b[S(z_o-d)-S(z_o+d)] + \mathrm{sgn}(z-z_o-d)e^{-bB|z-z_o-d|} \cdot [X \sin(BX|z-z_o-d|) + b\cos(BX|z-z_o-d|)] - \mathrm{sgn}(z-z_o+d)e^{-bB|z-z_o+d|} \cdot [X\sin(BX|z-z_o+d|)+b\cos(BX|z-z_o+d|)] + e^{-bB(z+z_o+d)}(X\sin[BX(z+z_o+d)] + b\cos[BX(z+z_o+d)]) - e^{-bB(z+z_o-d)} \cdot (X\sin[BX(z+z_o-d)]+b\cos[BX(z+z_o-d)]) \Big\} \tag{4.13}$$

where

$$A = \frac{gbQ_o}{2c_pT_oN^2}, \qquad B = \frac{Nt}{X^2+b^2}.$$

The symbol S and sgn denote the step function and the sign function, respectively. The above equation is an extension of the result of Raymond (1983) as it allows a heating distribution of finite width and height and includes the advection effect of a constant basic wind. The last two terms, which include $z+z_o+d$ and $z+z_o-d$, are the effects of wave reflection from the lower boundary. If these two terms are excluded, the response of the unbounded fluid to a heat source distributed in a layer of finite depth has the form of a region of mostly upward displacements drifting with the basic wind.

The vertical displacement at the center of the heating layer, z=0, in the unbounded fluid can be written

$$\hat{\eta} = \left(\frac{1}{\hat{x}^2+1}\right) \left\{ 1 - \exp\left(\frac{-\hat{t}}{\hat{x}^2+1}\right) \left[\hat{x}\sin\left(\frac{\hat{t}\hat{x}}{\hat{x}^2+1}\right) + \cos\left(\frac{\hat{t}\hat{x}}{\hat{x}^2+1}\right)\right] \right\}, \tag{4.14}$$

where the nondimensional variables are defined as

$$\hat{x} = \frac{x-Ut}{b}, \quad \hat{t} = \frac{Ndt}{b}, \quad \hat{\eta} = \frac{c_pT_oN^2}{gQ_o}\eta(x,0,t). \tag{4.15}$$

We are interested in two regions: (a) the region of the drifting heated air and (b) the region of the initial heating. Fig. 19a shows the vertical displacement around the center of drifting disturbance at different times in a reference frame moving with the basic

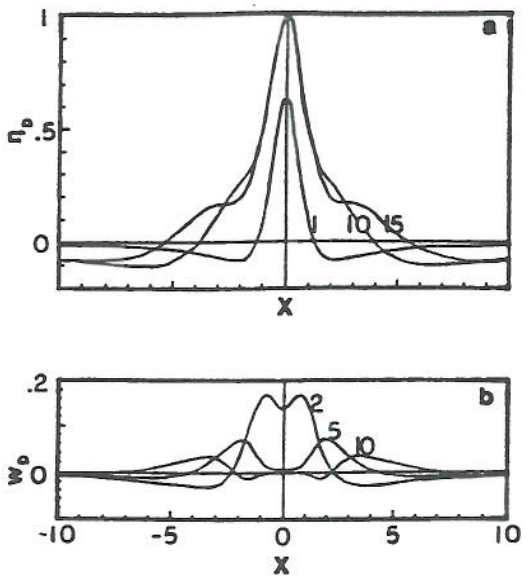

Fig. 19: (a) The vertical displacement at the center of the pulse heat source in a reference frame moving with the basic flow. The solution is given by Eq.(4.14). Notice that the strong updraft at the drifting center is accompanied by weak downdrafts on both sides. (b) The vertical velocity corresponding to (a). The numbers indicate the nondimensional times. (From Lin and Smith, 1986)

wind. The early response of the fluid to the heating is an upward displacement at the drifting center and downward displacements to the upstream and downstream sides of the growing disturbance. The weak downward displacements are necessary for compensating the upward motion at the center as required by the mass continuity even though that air was also heated by the wings of the pulse. Once the updraft at the drifting center weakens, the fluid in the adjacent regions can rise. By letting $\hat{x}=0$ in (4.14), the equation reduces to the growth function

$$\hat{\eta}_D = 1 - e^{-\hat{t}} \tag{4.16}$$

As $\hat{t}\to\infty$, Eq. (4.14) becomes

$$\hat{\eta}_D(\infty,x,z) = \frac{1}{\hat{x}^2+1}, \quad \text{for } z_o-d < z < z_o+d \tag{4.17}$$

which is everywhere proportional to the total amount of heat received by that air parcel. Fig. 19b shows the nondimensional vertical velocity which corresponds to Fig. 19a. This is obtained by taking the time derivative of Eq. (4.14),

$$\hat{w}_D = \frac{1}{(\hat{x}^2+1)^2}\exp\left(\frac{-\hat{t}}{\hat{x}^2+1}\right)\left[2\hat{x}\sin\left(\frac{\hat{t}\hat{x}}{\hat{x}^2+1}\right) - (\hat{x}^2-1)\cdot\cos\left(\frac{\hat{t}\hat{x}}{\hat{x}^2+1}\right)\right] \tag{4.18}$$

The updraft at the drifting center is accompanied by downdrafts on both sides in the early stages. At later times, two updrafts develop and propagate outward. This is analogous to the left and right moving waves in a two-dimensional shallow water system. These updrafts will overcome the downward displacement produced earlier and generate upward displacement at later times, as can be seen from Fig. 19a. At this time, the original disturbance has split in two.

For the flow response at the origin of the initial heating, the solution can be obtained by setting x=(in $\hat{x}$ in (4.14). The nondimensional form of the vertical displacement can be written as

$$\hat{\eta}_o = \frac{1}{(\hat{t}^2+1)}\left\{1 - \exp\left(\frac{-\hat{t}}{F(\hat{t}^2+1)}\right)\left[\hat{t}\sin\left(\frac{\hat{t}^2}{F(\hat{t}^2+1)}\right) + \cos\left(\frac{\hat{t}^2}{F(\hat{t}^2+1)}\right)\right]\right\} \tag{4.19}$$

where F is the Froude number associated with the thermal forcing, defined as U/Nd. A similar number has been used in Thorpe et al. (1980). Notice that the response of the flow at x=0 is strongly dependent on F and changes sign at $F=1/n\pi$. With a shallow

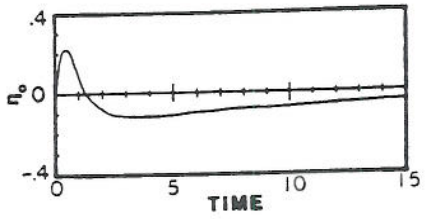

Fig. 20: The time evolution of nondimensional vertical displacement at the origin of the pulse heating. The solution is given by Eq. (4.19). The response is an upward displacement followed by a downward displacement, as the heated air drifts away. (From Lin and Smith, 1986)

heating, the Froude number is always greater than $1/\pi$. Thus, the vertical displacements near the origin of the heating have the same sign. Eq. (4.19) indicates that $\hat{\eta}_o$ decays as $1/\hat{t}$ as $\hat{t} \to \infty$ (Fig. 20). The response of the flow at the origin of pulse heating is an upward displacement followed by a downward displacement, as the heated air drifts away. The downward displacement produced at later times is associated with the compensating downdraft as the growing updraft drifts downstream. Raymond (1986) has investigated the flow response to a prescribed steady heat source for a wide variety of Froude numbers.

4.2 Flow response to a steady heating

As mentioned earlier, studies of steady heating in a moving atmosphere in connection to orographic rain (Smith and Lin, 1982), heat islands (Fig. 25; Garstang et al., 1975; Mahrer and Pielke, 1976) and thunderstorm downdrafts (Thorpe et al. 1980) showed a curious negative relationship between heating and vertical displacement. That is, a downward (upward) displacement in the vicinity of the heat source (sink) is produced by the heating (cooling). This result is directly related to the steadiness of the heating (Smith and Lin, 1986; Bretherton, 1988) and will be explained below.

The vertical displacement of a moving stratified fluid to a pulse of point heat source may be obtained by taking b --> 0 and keeping bQ_o constant in Eq. (4.12),

$$\eta(t, x, z) = \frac{-q_o t}{2\pi N X^2} \cos\left(\frac{Nzt}{X}\right) \tag{4.20}$$

where $q_o = bQ_o$, and $X=(x-Ut)/b$. The above equation is identical to Eq. (3) of Bretherton (1988). Fig. 21 shows the vertical displacement at time t after a localized impulsive buoyancy source is imposed at

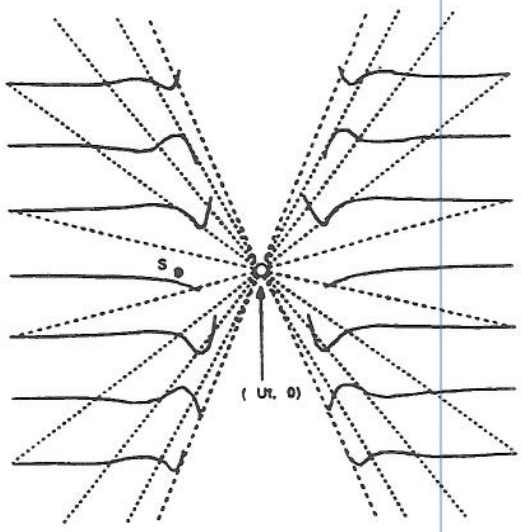

Fig. 21: The vertical displacement at time t after a localized impulsive buoyancy source is imposed at t=0 in a stratified fluid. The dashed lines are the nodal lines $z=(n+1/2)\pi X/Nt$ on which there is no vertical displacement. The solid lines are dye lines that were initially horizontal and have been displaced in response to the source. (From Bretherton, 1988).

t=0 in a stratified fluid. Since we are interested in the response near the origin of the heating (x=z=0), the above equaiton reduces to

$$\eta(t, 0, 0) = \frac{-q_o}{2\pi N U^2 t} \quad (4.21)$$

The steady state heat source may be regarded as a succession of very short heat pulses. Thus the vertical displacement at the origin of the heating can be obtained by the Green's function method which amounts to integrating Eq. (4.21) with respect to time

$$\eta(t, 0, 0) = \int_0^t \eta(t-\tau, 0, 0)\, d\tau = \int_0^t \eta(T)\, dT \approx \int_{\Delta x/U}^t \eta(T)\, dT = \frac{-q_o}{2\pi N U^2} \ln\left(\frac{tU}{\Delta x}\right) \quad (4.22)$$

where Δx is a characteristic horizontal distance such that $\Delta x<Ut$. The contribution to the displacement from times less than $\Delta x/U$ is assumed to be negligible (Bretherton, 1988). Therefore, the vertical displacement grows logarithmically and negatively at the origin of the heat source. The vertical displacement for the steady heating which is distributed horizontally and vertically can also be obtained by integrating Eq. (4.13) with respect to time.

An alternative way to explain this phenomenon is by considering the energy budget. The linearized steady state energy equation may be derived by introducing the relation, $\theta'/\theta_o \sim -\rho'/\rho_o$, (which may be obtained by linearization and combination of Poisson's equation and the equation of state for an ideal gas) in Eq. (2.16) and excluding the basic shear terms,

$$\frac{\partial}{\partial x}(EU + p'u') + \frac{\partial}{\partial z}(p'w') = -\frac{g^2}{c_p T_o N^2}\rho' q' \quad (4.23)$$

where $E=0.5\rho[u'^2 + (g\rho'/N\rho_o)^2]$ is the perturbation wave energy in a hydrostatic atmosphere. According to the above equation, in order to add the thermal energy to the system the steady heating must be added where the air density is low, i.e. at high temperature. This implies that the perturbation flow field must adjust itself so that the regions of negative density anomaly (negative displacement) receive the heat.

Using a group velocity argument, Bretherton (1988) indicates that the t^{-1} dependence of η is a geometrical effect, which relies only on the fact that there are wavenumbers with zero group velocity around which there is a finite rate of dispersion. The small, but nonzero, group velocities of nearby wavenumbers spread their energy into a region of space that expands linearly with time in each direction, so that the energy density, a quadratic function of η, decreases as t^{-2}. The vertical displacement of the fluid to a maintained heat source grows logarithmically since the displacements produced by individual heat pulses are all in phase at the origin of the heating. Notice that the waves of zero group velocity also have zero frequency.

Since the vertical displacement grows logarithmically near the origin of the steady heat souce, the flow must undergo a permanent change, instead of a localized steady state response. As discussed by Smith and Lin (1982), this is due to the fact that a net amount of heat has been received by the airstream. To avoid this net heating problem, Smith and Lin have shown that a steady state response will occur if the horizontally integrated heating is zero. Bretherton (1988) extended Smith and Lin's result to a more general criterion. He proved that if a steady buoyancy source $q'(x,z)$ is turned on at t=0, then a finite, steady displacement field $\eta(x,z)$ will set up only when

$$\int_{-\infty}^{\infty} q'(x,z)e^{\pm iNz/U}\,dx\,dz = 0 \tag{4.24}$$

That is, when there is no projection of the heat source on the wavenumbers $\pm k_0=(0,\pm N/U)$ corresponding to the ω^+ and ω^- modes which have zero group velocity. The $\omega^\pm$ modes denote the internal gravity waves which have frequencies of $Uk\pm Nk/m$ and group velocities of $c_g^{\pm}(k)=(U\pm N/m, -Nk/m^2)$.

The gravity waves produced by a pulse heating in an unsheared flow are symmetric about its center and impart no net momentum flux to the flow. Thus, there are no vertically propagating gravity waves produced. However, vertically propagating gravity waves can be generated by a steady heating or cooling. Similar to Eq. (4.22), the vertical displacement for the steady state heating can be obtained by integrating Eq. (4.13) with respect to time

$$\eta(t,x,z) = \int_0^t \eta(t-\tau, x, z)\,d\tau \tag{4.25}$$

Fig. 22 shows an example in which a heat source concentrated in the stippled region is given by a Heaviside function at t=0 in an unbounded stratified fluid. The solution is given by Eqs. (4.25) and (4.13) by excluding the lower boundary reflections (i.e., the last two terms in (4.13)). The integrand in Eq. (4.25) is computed numerically using Simpson's rule. The response of the fluid has two separate parts. First, there exists a region of upward displacement generated initially at the origin of the heat source and which is subsequently advected downstream by the basic wind. The amplitude of the displacements keeps growing with time. Notice that the peak of the upward displacement appears to propagate downstream with a slower speed (~0.7U) than the basic flow. The upward displacement is a

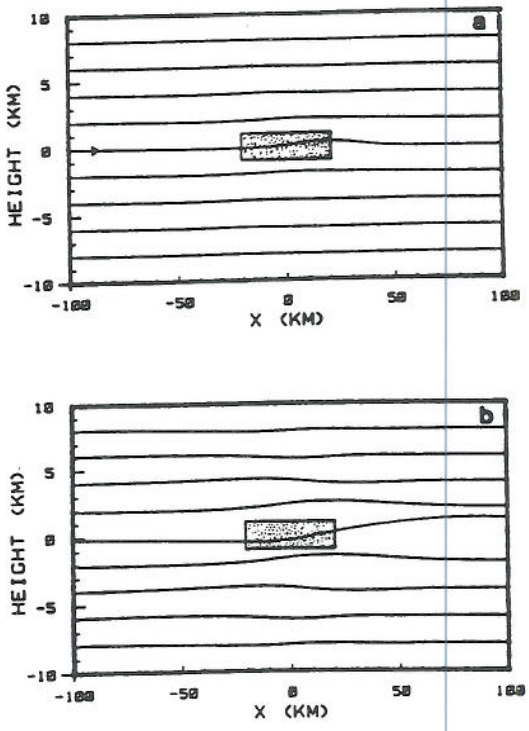

Fig. 22: Vertical displacement of a hydrostatic atmosphere to a steady heating (stippled) imposed at t=0. The solution is given by Eqs. (4.25) and (4.13), excluding the lower boundary reflections (the last two terms), with U=10 ms^{-1}, N=0.01 s^{-1}, T_o=273 K, Q_o=1 J kg^{-1} s^{-1}, b=20 km, d=1 km, and z_o=0 km. (From Lin and Smith, 1986)

superposition of an infinite number of individual elements corresponding to individual pulse heating separated by infinitesimal time intervals. In addition, there is a downward displacement in the vicinity of the stationary source, which develops at a much slower rate than that of the drifting disturbance. The corresponding vertical momentum fluxes are shown in Fig. 23. There exists a layer of negative (positive) momentum flux above (below) the heating layer. The magnitude of the momentum flux increases as

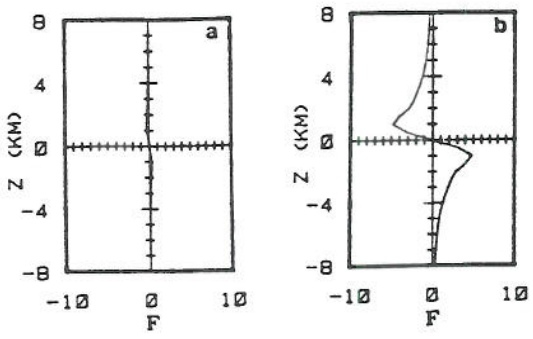

Fig. 23: The corresponding vertical momentum fluxes for the flow fields of Fig. 22. The units of the momentum flux are 10^4 Newton m^{-1}.

the gravity wave associated with the steady heating becomes stronger and propagates to higher (lower) layers. In the upper layer, the downward transport of momentum is a consequence of the upstream phase tilt of the vertical displacement, which gives a greater horizontal perturbation velocity in the downward motion. This is similar to the mountain wave theory (Eliassen and Palm, 1960). The convergence of momentum flux at the heating level must act to accelerate the flow slowly (as a second-order quantity) there while air above and below is decelerated.

4.3 Applications

a. Flow over a heat island

The above theory has been applied to the problem of stratified flow over a heat island by Lin and Smith (1986). This helps to explain the downward displacement observed over a heated island and upward displacement on the downstream side (Fig. 25; Malkus, 1963; Garstang et al., 1975). Figure 24 shows the disturbance generated by a stationary heat source (stippled region) introduced at an initial time, t=0, in a hydrostatic atmosphere over a flat surface. The heating represents the low-level sensible heating

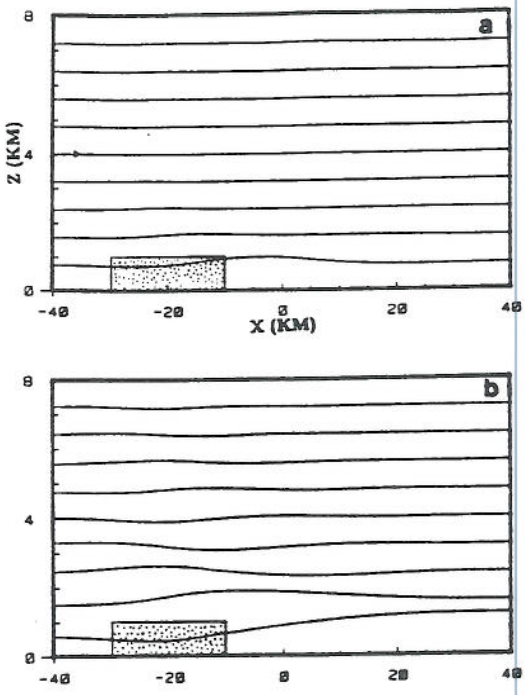

Fig. 24: Vertical displacement for an airflow over a heat island. The stationary heat source is concentrated in the stippled region. This flow is given by Eq. (4.25) with U=5 ms^{-1}, N=0.01 s^{-1}, T_o=273 K, Q_o=0.35 J kg^{-1} s^{-1}, z_o=0.5 km, b=10 km, d=0.5 km and c=20 km. Two times are shown (a) 5000 s, and (b) 20000 s. (From Lin and Smith, 1986)

caused by a heated island in the daytime. For the heating rate, we consider a simple case of a heat island which warms 10 K from 0600 to 1400 LST. For simplicity, we assume that the heating extends uniformly to the top of the boundary layer, say 1 km. The heat flux thus calculated is approximately 348 J m^2 s^{-1}. This gives a heating rate of 0.35 J kg^{-1} s^{-1}. The response of the fluid to the low-level heating is similar to the case in Fig. 22 in that heating correlates with negative displacement. The dynamics is essentially the same as explained in Section 4.2.

Notice that the air parcel ascends on the downwind side of the heat island. Figure 25 shows the divergence and vertical velocity fields over Barbados (DeSouza, 1972; summarized in Garstang et al., 1975), which indicates that there exists a downward motion over the island and an upward motion downwind during the day. Rainfall enhancement is often observed on the downwind side of metropolitan areas, such as St. Louis (Fig. 1; Braham and Dungey, 1978; Changnon, 1981). This phenomenon is often explained by the addition of condensation nuclei which are swept downstream when air flows past an urban heat island. A study of the combined effects of the addition of condensation nuclei in the region of ascending motion downstream of an urban heat island may provide a better explanation of the phenomenon. A similar phenomenon has also been obtained in linear studies of Hsu (1987b) and Luthi et al., 1989) and in the nonlinear numerical study of Hjelmfelt (1982).

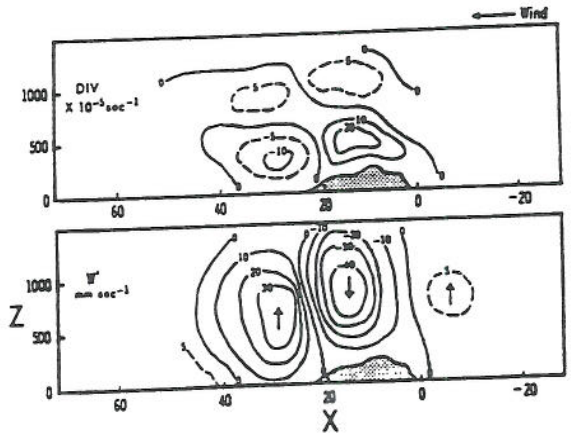

Fig. 25: Divergence and vertical velocity fields over Barbados during the summers of 1968 and 1969 during the day. The horizontal and vertical distance units are in km and m, respectively. (From Garstang et al., 1975, after DeSouza, 1972)

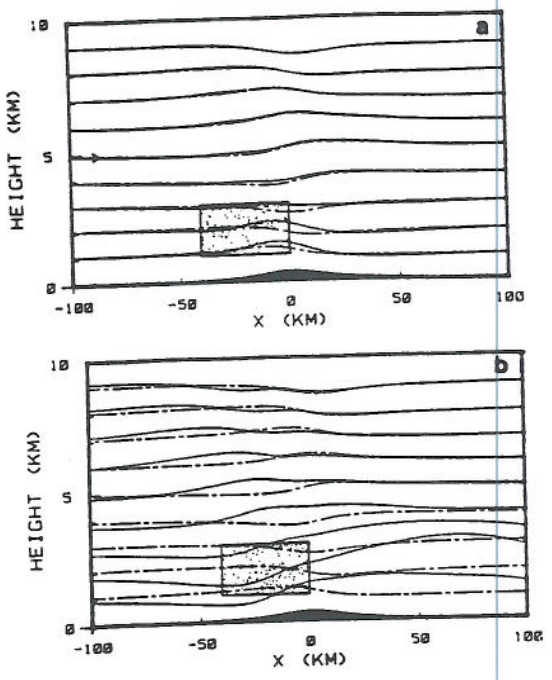

Fig. 26: Hydrostatic vertical displacement generated by a mountain and an elevated heat source (stippled) imposed at t=0. The solution is given by Eqs. (3.44c), (4.13) and (4.25) with U=10 ms^{-1}, N=0.01 s^{-1}, T_o=273 K, Q_o=1 J kg^{-1} s^{-1}, b=20 km, d=1 km and c=20 km, a=20 km, h_o=400 m. The dashed lines represent the vertical displacement of the adiabatic mountain waves. Two times are shown: (a) 3000 s, and (b) 13000 s. The heating corresponds to a precipitation of 2.5 mm h^{-1}. (From Lin and Smith, 1986)

b. Orographic rain

Figure 26 shows an example in which the heating is associated with a stationary precipitating upslope orographic cloud in a hydrostatic atmosphere. The solution is obtained by superimposing the mountain induced wave (Eq.(3.44c)) and the heat induced wave (Eq.(4.25)). The dry mountain wave solution

is also plotted for comparison. The heating rate corresponds to a rainfall rate of about 2.5 mm h^{-1}. The heating is concentrated in the stippled region and activated at t=0 s. After some time, the thermally generated disturbance has grown and drifted downstream. This displacement keeps growing as the stationary heating continues and reaches considerable magnitude by 13,000 s≈3.6 hrs (Fig. 26b). If the heating continues for some time, a negative displacement is produced in the vicinity of the upslope orographic cloud. This phenomenon was found by Smith and Lin (1982) and is explained more completely here. In the real atmosphere, broad upslope rain may be limited by the heat induced descent either in durartion or intensity. This result has some similarities to a number of studies of mountain waves and orographic rain (e.g., Raymond, 1972; Fraser et al., 1973; Barcilon et al., 1980). The vertical transport of the horizontal momentum is convergent at the heating layer, which is similar to the case of an unbounded fluid (Fig. 23) with the modification of orographic effects. With certain realistic values of the parameters U, N, Q_o, b, d, and z_o, a positive momentum flux below the heating layer is produced implying a reverse of the mountain drag as discussed in Smith and Lin (1982) and Durran and Klemp (1982).

To avoid the addition of latent heat in a region of downward motion, Lin (1986b) adopts a simple rain parameterization in a linear, finite-element numerical model. The diabatic heating is parametrized by

$$q' = \left(\frac{c_p T_o N^2}{g}\right) \varepsilon w' \alpha(w,\eta), \tag{4.26}$$

where

$$\varepsilon = 1 - \frac{N_w^2}{N^2}, \quad N^2 = \frac{g}{T_o}(\Gamma_d - \Gamma), \quad N_w^2 = \frac{g}{T_o}(\Gamma_s - \Gamma),$$

$$\alpha(w,\eta) = 1 \quad \text{if } w>0 \text{ and } \eta>0,$$

$$\alpha(w,\eta) = 0 \quad \text{otherwise}. \tag{4.27}$$

In the above formulation, the cloud forms immediately in a region of upward velocity and displacement and falls to the surface immediately in a region of downward velocity or displacement. This parameterization of a precipitating cloud is similar to that used by Fraser et al. (1973) and Barcilon et al. (1980). The parameter ε can be as small as 0.2 in the cold air (Barcilon et al., 1980). Eq. (4.26) may be substituted into the thermodynamic equation, Eq. (2.13), with the terms of V, U_z and V_z excluded to obtain

$$\frac{\partial \theta'}{\partial t} + U\frac{\partial \theta'}{\partial x} + \frac{N^2 \theta_o}{g}(1-\varepsilon\alpha)w' = 0. \tag{4.28}$$

The parameter α will be greater than or equal to zero depending upon whether the point of interest is inside or outside the cloud. The air parcel follows a moist adiabat if it is inside the cloud and a dry adiabat if outside the cloud.

Figure 27 shows the numerical results of orographic rain in a stable atmosphere with ε=0.8. The stability parameter (ε) is approximately equal to an actual lapse rate of 6.25 K km^{-1} with a moist lapse rate of 7 K km^{-1}. The incoming airstream is saturated and the moisture is limited to the lower 6 km. The parameterization is turned on at 10,000 s. Four time steps are shown to indicate the time evolution of the flow. The heating regions are outlined, which may represent the cloud boundaries. At 30,000 s, two drifting clouds appear to the downwind side of the mid- and low-level stationary clouds. These drifting clouds originate and subsequently separate from the stationary clouds. The flow reaches a steady state locally in the vicinity of the mountain at later times as shown in Fig. 27d. The local features of the low-level stationary cloud are similar to those found by Barcilon et al. (1980).

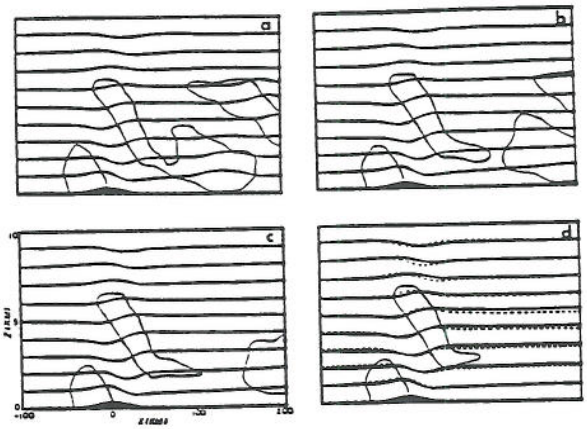

Fig. 27: Streamlines and heating regions of precipitating orographic clouds in a stable atmosphere with ε=0.8 simulated by a linear, finite element model. Other parameters of the flow are U=10 ms^{-1}, N=0.01 s^{-1}, T_o=273 K, and ρ_o=1 kg m^{-3}. The flow is directed from left to right. The mountain height and half-width are 400 m and 20 km, respectively. The dotted lines in (d) are the corresponding dry mountain waves. Four time steps are shown: (a) 30000 s, (b) 40000 s, (c) 50000 s, and (d) 60000 s. (From Lin, 1986b)

The two stationary clouds at the lower and middle levels may be interpreted as local quasi-stationary heat sources. According to the finding of Smith and Lin (1982), the phase relationship between the stationary heating and the heat-induced vertical displacement in the flow parameters chosen here is negative. However, the orographic lifting acts to support the existence of the stationary clouds. In short, the two stationary clouds in Fig. 27d are supported by the orographic forcing and limited by the long-term heating generated by the clouds themselves. The corresponding dry mountain wave is plotted (dotted lines) against the moist flow (Fig. 27d). In general, the streamlines are depressed upstream in the lower layer (e.g., z=2 km) and lifted downstream in the middle layer (e.g., z=4 km) by the presence of moisture.

Barcilon and Fitzjarrald (1985) investigated the nonlinear effects on a precipitating orographic cloud using a theoretical approach and a similar rain parameterization of Eq. (4.26). They found that the nonlinearity and lower boundary affects the dynamics of mechanically and thermally induced waves and wave drag. The wave drag depends upon: (1) the location of the moist layer with respect to the ground, (2) the amount of moisture, (3) the degree of nonlinearity and (4) the asymmetry in the bottom topography. For symmetrical mountain profiles, substantial drag reductions are obtained when the moisture is adjacent to the topography. In addition, an increase in the nonlinearity increases the drag.

c. Moist convection

The maintenance of a quasi-steady squall line remains an unsolved dynamical problem. One may regard the evaporative cooling in the subcloud layer produced by the precipitation falling from the updraft aloft as a stationary heat sink in the reference frame of the moving line. The steady state assumption for the cooling in a squall-line type of thunderstorm is not an unreasonable one (Lilly, 1979). Figure 28 shows an example of an airflow over a stationary heat sink. In a moving frame, the stationary heat sink may be regarded as a left-moving squall line. The propagation speed of the heat sink is 15 ms^{-1} and the Froude number (U/Nd) is 1.5. In the vicinity of the heat sink, the air is displaced downward at first and then upward. The approach to steady state is essentially the same as in the flow over a heat source but in an opposite way. The local features near the heat sink are similar to the steady state solutions of Thorpe et al. (1980) and Lin and

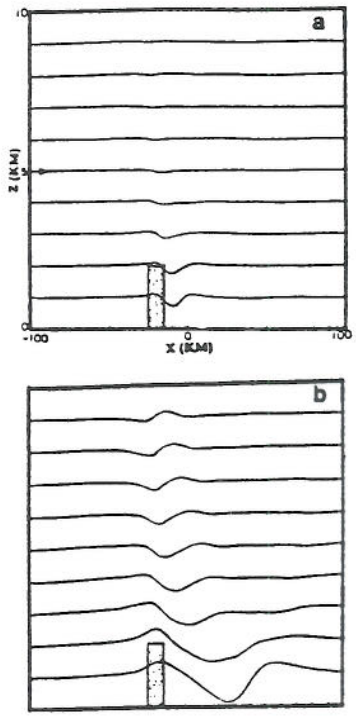

Fig. 28: Vertical displacement near a stationary heat sink representing evaporative cooling under a precipitating cloud. This flow is given by Eqs. (4.25) and (4.13) with U=15 ms^{-1}, N=0.01 s^{-1}, Q_o=-4 J kg^{-1} s^{-1}, z_o=1 km, b=5 km, d=1 km and c=20 km.. Two times are shown: (a) 1000 s, and (b) 4000 s. (From Lin and Smith, 1986)

Smith (1986). The phase relationship between the evaporative cooling and the induced vertical displacement in the region near the heat sink is negative, as shown earlier. The upstream tilt of the vertical displacement indicates the upward propagation of the generated internal gravity waves. In addition, there is a region of positive displacement propagating downstream kinematically, which is similar to the heating case studied earlier.

The positive displacement in the vicinity of the heat sink resembles the flow strucure near the gust front of a squall line and may provide a possible mechanism for the maintenance of a squall line. Robustness of this result can be demonstrated by solving the same problem with a linear finite-element numerical model (Lin, 1986b). This is also a convenient way to exhibit other aspects of flow field as all of the flow variables are computed by the model. Figure 29 shows that the vertical displacement, perturbation fields of the density, horizontal velocity and vertical velocity at 4000 s. The field of vertical displacement produced by the numerical model (Fig. 29a) is slightly smoother than that of the analytical solution (Fig. 28b) because a numerical smoothing technique is applied in the model to avoid the spurious growth of high wave number modes. In general, the agreement between

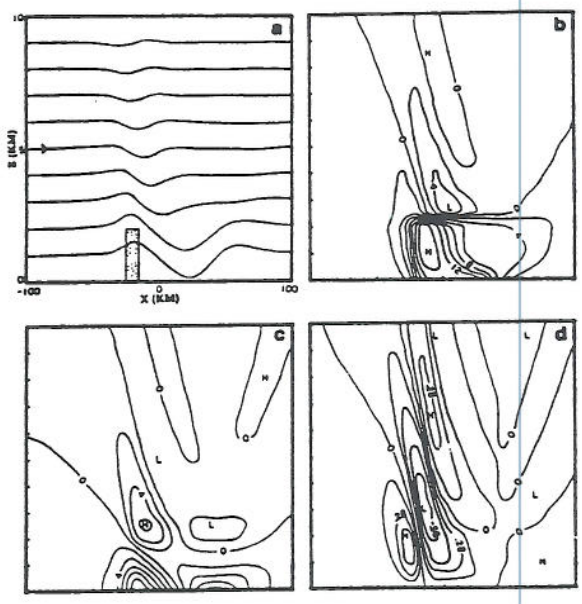

Fig. 29: Airflow near a stationary heat sink simulated by a numerical model at 4000 s. The parameters are same as those in Fig. 28: (a) vertical displacement, (b) perturbation density, (c) horizontal perturbation velocity, and (d) vertical velocity. (From Lin, 1986b)

the numerical model and analytical results is good. The density field (Fig. 29b) shows that there exists a pool of cold air near the stationary heat sink. The sharp density difference in front of the heat sink (x=-35 km) may be regarded as an upstream gust front produced by the density current. The high density region may correspond to the mesohigh as often observed under the strong downdraft region. On the downwind side, the cold air is advected more dispersively, i.e., the density difference is not as sharp as on the upstream side. From the velocity fields (Fig. 29c,d), there exists upstream motion and a region of surface convergence in front of the stationary heat sink. This is consistent with the finding of the positive displacement near the heat sink (Fig. 28). With application to the low-level flow associated with a squall line, the upward motion and low-level convergence may play an important role in generating a new convective area on the upstream side of the moving squall line. This is consistent with the nonlinear numerical results of Rotunno et al. (1988), in which new cells of the squall line system keep developing along the gust front, which helps to explain the maintenance of a squall line.

Raymond (1986) solved a similar two-dimensional initial value problem with both prescribed condensational heating and evaporative cooling considered. The strong speed selectivity of wave-CISK is explained as a constraint in which the actual vertical velocity at the level of free convection must exceed the diabatic mass flux there. The solution, however, proposes a potential problem within the wave-CISK formalism. Though a moving region of heating can indeed produce upward motion at the level of free convection, upstream subsidence makes it doubtful that sufficient net upward displacement of low-level air can be generated by this mechanism. This problem is alleviated when the evaporative cooling associated with precipitation is present. The subsidence generated by the heating can be canceled by the lifting generated by the cooling. This lifting is also shown in Figs. 28 and 29.

Nicholls et al. (1991) considered a special case of Lin and Smith (1986), in which the basic state atmosphere is quiescent and bounded above by a rigid top. There exists two modes in the flow: (1) a deep fast-moving mode which is responsible for subsidence warming throughout the depth of troposphere; (2) a slower moving mode which corresponds to midlevel inflow and lower- and upper-level outflows. They also obtained an analytical solution for a pulse forcing in a flow topped by a rigid lid. The solution shows a result similar to that of Lin and Goff (1988), in which two symmetric waves propagate outward from the origin of initial heating. The structure of these propagating waves is similar to gravity waves produced in two-dimensional numerical simulations of convection occuring over the Florida penninsula.

d. Gravity waves on inversions

The generation mechanism of internal gravity waves on a low-level inversion by a thunderstorm has been proposed by Lin and Goff (1988). The model described in the last section (Smith and Lin, 1982) and in this section (Lin and Smith, 1986) may be modified to include: (1) a sharp temperature inversion, (2) a quiescent basic state, and (3) a height dependency of the Brunt-Vaisala frequency. Thus, Eq. (4.1) becomes

$$w'_{ttzz} + N^2(z)\, w'_{xx} = \frac{g}{c_p T_o} q'_{xx}, \tag{4.29}$$

where N(z) and q'(t,x,z) are represented by

$$N(z) = N\,[\delta(z) + S(z)], \qquad -H \le z \tag{4.30}$$

$$q'(t,x,z) = \frac{Q_o b^2}{x^2 + b^2}\,\delta(t)\,\delta(z-z_1), \qquad z_1 > 0 \tag{4.31}$$

where S is a step function. Notice that the surface is located at z=-H. In Eq. (4.30) we assume a sharp temperature inversion riding on a neutrally stratified layer of depth H. The Brunt-Vaisala frequency is constant in the upper layer above the inversion (z>0). The heating is released instantly as a pulse located at $z=z_1$.

The problem is solved by determining the relevant Green's function, as described earlier. Taking Fourier transforms in t and x of Eqs. (4.29) and (4.31) gives

$$\hat{w}_{zz} + \left(\frac{Nk}{\omega}\right)^2 \hat{w} = \frac{gQ_o b k^2}{4\pi c_p T_o \omega^2}\, e^{-b|k|}\,\delta(z-z_1) \tag{4.32}$$

The lower and upper boundary conditions are $\hat{w}=0$ at z=-H and $\hat{w}\sim\exp(iN|k|/\omega)$ as z --> ∞, respectively. There are four interface conditions across the interface. Across the interface $z=z_1$, $\hat{w}$ is continuous. Integrating Eq. (4.32) across the interface yields another condition that $\hat{w}_z$ is continuous. Likewise, at the inversion z=0, $\hat{w}$ is continuous and integrating Eq. (4.32) across the inversion yields a condition which relates to the strength of the inversion; that is, $g'=g\Delta\theta/\bar{\theta}$ (Geisler and Bretherton, 1969). The solution in the lower layer (-H<z<0) is given by

$$\eta = \frac{igQ_o b(z+H)}{4\pi c_p T_o} \int_{-\infty}^{\infty} k^2 e^{(-b|k|+ikx)} dk \int_{-\infty}^{\infty} \frac{e^{i(Nz_1|k|/\omega+\omega t)}}{\omega(\omega^2 - iNH\omega|k| - g'Hk^2)}\, d\omega \,, \tag{4.33}$$

where the vertical displacement is defined as $\partial\eta/\partial t = w$. A closed form for the above equation is possible but is the algebra is tidious. An asymptotic nondimensional form is obtained by applying the method of stationary phase (see Appendix A of Lin and Goff, 1988) for large t and x

$$\eta = \frac{-(z+1)Q_o t^2 e^{-Mt/x^2}}{2|x|\left[(x^2-t^2)^2 + (Ftx)^2\right]} \cdot\left[(x^2-t^2)\sin(Mt/|x|) + Ftx\cos(Mt/|x|)\right] \tag{4.34}$$

The variables x, z, η, t and Q_o are nondimensionalized by b, H, H, b/c_o and $c_p T_o c_o^2/g$, respectively, where c_o is the linear internal shallow water phase speed, i.e. $\sqrt{g'H}$, which is related to the strength of the inversion. The two nondimensional numbers M and F are defined as Nz_1/c_o and NH/c_o, respectively. The parameter F represents a heating-induced Froude number defined by Lin and Smith (1986). A similar result can be obtained for a case of a neutrally stratified layer overriding a stable layer of depth H with no inversion in between. Instead of $\sqrt{g'H}$, the linear internal shallow water phase speed (c_o) becomes $2NH/\pi$ (e.g., see Case IIIA of Grimshaw, 1981).

Figure 30a shows a case with M=0.1, F=1, and Q_o=0.5, and the dimensional parameters H=5500 m, z_1=550 m, c_o=55 m s^{-1}, and N=0.01 s^{-1}. Four time steps are shown in the figure. Since the forcing produces both right- and left-moving waves symmetrically, only the right-moving wave is plotted. In this case, a wave of depression is produced by the latent heating. The gravity wave is dispersive and decays gradually. If the nonlinear effect is included, a solitary wave of depression may result due to the balance between the competing effects of wave steepening and frequency dispersion. In this way, the wave is able to retain its identity as an isolated quasi-steady disturbance of permanent

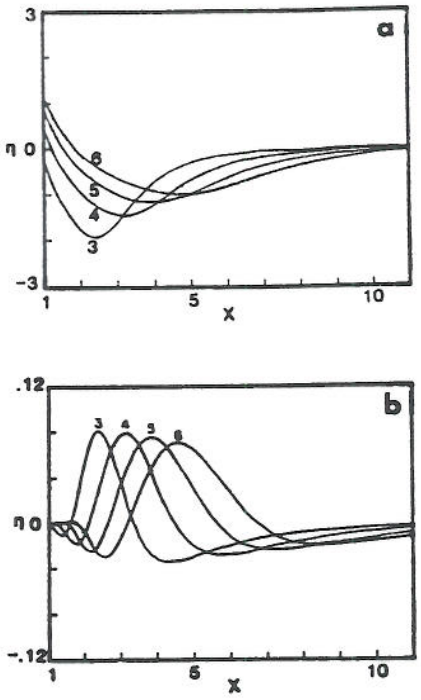

Fig. 30: Gravity wave generated on an inversion: (a) The vertical displacement at the inversion level (z=0) with M=0.1, F=1, and Q_o=0.5 for t=3, 4, 5, 6. (b) same as (a) except with M=2, and F=1. The solution is given by Eq. (4.34). (From Lin and Goff, 1988)

form when it propagates a long distance from the origin. Mesoscale solitary waves of depression with wavelength on the order of 100 km have been observed in the atmosphere (e.g., Pecnick and Young, 1984; Lin and Goff, 1988). The generation mechanism considered here may also lead to a favorable circumstances for the creation of wave of elevation on a low altitude inversion. Fig. 30b shows an example with M=2, F=1 and the dimensional parameters H=100 m, z_1=2000 m, c_o=10 m s^{-1}, and N=0.01 s^{-1}. An initial long wave disturbance of this type may evolve into a finite number of amplitude-ordered solitary waves of elevation followed by a relatively weak wave train if the nonlinear effect is included. This type of solitary wave of elevation with wavelength on the order of 10 km has been observed in the atmosphere (e.g., Abdullah, 1955; Christie et al., 1978). The well-known morning glory observed in Australia belongs to this type of wave.

In addition to the above propagation mechanism for mesoscale waves, linear waves may be able to propagate a long distance if there exists a wave duct in the atmosphere. Lindzen and Tung (1976) showed that a stable wave duct adjacent to the surface must be capped by an unstable layer which contains a critical level. It is also noteworthy to mention that mesoscale waves may be generated by other mechanisms, such as shear instability (Gossard and Hooke, 1975; Stobie et al., 1983), geostrophic adjustment (House, 1961; Kaplan and Paine, 1977; Uccellini et al., 1984; Koch and Dorian, 1988; reviewed by Uccellini and Koch, 1987), in addition to convection (Wagner, 1962; Feguson, 1967; Bosart and Cussen, 1973; Lin and Goff, 1988).

5. Shear Flow over a Meso-γ Scale Heat Source

As discussed in the introduction, diabatic heating in a flow with vertical shear is a common element in various mesoscale circulations (e.g., Lin, 1987). The mathematical problem of adiabatic perturbations to a shear flow in a stably stratified fluid has been studied extensively in the last three decades. Bretherton (1966) found that the vertical wavenumber becomes large and that the group velocity becomes more horizontally oriented as the critical level is approached. Booker and Bretherton (1967) found that the gravity waves are attenuated exponentially as they pass through a critical level at which the horizontal basic wind is equal to the

horizontal phase speed if the Richardson number (Ri) is everywhere greater than 1/4, i.e. if the flow is dynamically stable. The horizontal momentum is transferred to the basic flow. The critical level problem in an adiabatic flow has been studied by several authors (see Gossard and Monk, 1975; Maslowe, 1986; LeBlonde and Mysak, 1978 for reviews). The response of a stably stratified shear flow with a critical level to a mountain (orographic forcing) has been studied by Smith (1984, 1986). The solutions have been applied to the lee cyclogenesis problem. The response to a diabatic heating has been studied by Lin (1987) and Lin and Chun (1991). The solutions have been used to explain the maintenance of a midlatitude squall line and the formation of density current associated with evaporative cooling.

Observations of large sheared cumulonimbus convection also suggested that the environmental wind relative to the storm movement often reverses its direction at some height (e.g., Newton, 1966; Marwitz, 1972). In order to understand the effects of latent heating associated with cumulonimbus convection on the environmental flow, it is important to study the three-dimensional response of both uniform and sheared stratified flows to diabatic heating. In solving the three-dimensional response to a prescribed elevated heating, representing the latent heating associated with isolated supercell thunderstorms, Lin (1986a) and Lin and Li (1988) proposed that the V-shaped cloud tops over severe storms (see Heymsfield and Blackmer, 1988 for a brief review) are formed by the thermally forced gravity waves.

5.1 Two-Dimensional Shear Flow with a Critical Level

The equation governing the two-dimensional steady-state, small-amplitude vertical velocity perturbation in a stratified, nonrotating, Boussinesq fluid with diabatic heating can be simplified from Eq. (2.15),

$$U^2\frac{\partial^2}{\partial x^2}(w'_{xx}+w'_{zz})-UU_{zz}w'_{xx}+N^2w'_{xx}=\frac{g}{c_pT_o}q'_{xx} \tag{5.1}$$

The homogeneous part of the above equation has been discussed in Bretherton (1966). To simplify the problem, we may assume that the flow is in hydrostatic balance and the basic wind shear is constant with height. After making the Fourier transform in x, the above equation becomes

$$\hat{w}_{zz}+\frac{N^2}{U^2(z)}\hat{w}=\frac{g}{c_pT_oU^2(z)}\hat{q} \tag{5.2}$$

In this section, we allow the basic wind to vanish at a certain height. This will introduce a singularity to the equation at the wind reversal level, which coincides with the critical level in a steady state flow. The Brunt-Vaisala frequency, N, is assumed to be constant with height and U(z) is given by

$$U(z) = \alpha z, \quad -H_o \le z, \tag{5.3}$$

where $\alpha=-U_o/H_o$, U_o is the basic flow at the surface, and H_o is the depth from the surface to the critical level. For convenience, the origin of the vertical coordinate is chosen to be at the critical level. The diabatic heating represents either low-level sensible heating or elevated latent heating, and is assumed to have the form

$$\begin{aligned} q'(x,z) &= Q_o f(x), && -H_o \le z < -H_1 \\ &= 0, && -H_1 \le z \end{aligned} \tag{5.4}$$

where H_1 may be positive or negative depending upon whether the top of the heating layer is below or above the critical level. Substitution of the Fourier

transform of the above equation into Eq. (5.2) yields

$$\hat{w}_{zz} + \left(\frac{N}{\alpha z}\right)^2 \hat{w} = \frac{gQ_o}{c_pT_o\alpha^2 z^2}\hat{f}(k), \quad -H_o \le z < -H_1$$
$$= 0, \quad -H_1 \le z. \tag{5.5}$$

The general solution of the above equation may be written

$$\hat{w}(k,z) = Az^{1/2+i\mu} + Bz^{1/2-i\mu} + \frac{gQ_o\hat{f}(k)}{c_pT_oN^2}, \quad -H_o \le z < -H_1$$
$$\hat{w}(k,z) = Cz^{1/2+i\mu} + Dz^{1/2-i\mu}, \quad -H_1 \le z \tag{5.6}$$

where

$$\mu^2 = Ri - 1/4, \quad Ri = N^2/\alpha^2. \tag{5.7}$$

The upper radiation condition and lower boundary condition requires C=0 (Booker and Bretherton, 1967) and $\hat{w}(z=-H_o)=0$, respectively. The interface conditions at $z=-H_1$ appear to be that both $\hat{w}$ and $\hat{w}_z$ are continuous across it. Applying the boundary and interface conditions to Eq. (5.6) leads to a solution of $\hat{w}(k,z)$ in Fourier space. A perturbation streamfunction ψ' may be defined as $-\partial\psi'/\partial x = w'$. The vertical displacement (η) is related to the perturbation streamfunction according to $\eta = -\psi'/U$ if $U \neq 0$. The total streamfunction can then be calculated by

$$\psi = \bar{\psi} + \psi' = \int_{-H_o}^{z} U(z)\,dz + \psi', \tag{5.8}$$

or

$$\psi = \left(\frac{U_oH_o}{2}\right)\left[1 - \left(\frac{z}{H_o}\right)^2\right] + \psi'. \tag{5.9}$$

Using a bell-shaped heating function with compensative cooling such as that in Eq. (3.50) one may obtain solutions in the physical space of the form

$$\psi' = \frac{Q_o}{Ri}\left[TNX\left\{\frac{z1s}{2}\left[(\cos T1 - \cos T2) - \frac{1}{2\mu}(\sin T1 + \sin T2)\right] + z0s\cdot\cos T3 - 1\right\} + LNX\left\{\frac{z1s}{2}\left[\frac{1}{2\mu}\cdot(\cos T1 - \cos T2) + (\sin T1 + \sin T2)\right] - z0s\cdot\sin T3\right\}\right]$$
$$-1 \le z < -H_1 \tag{5.10a}$$

$$\psi' = \frac{Q_o}{Ri}\left[TNX\left\{\frac{z1s}{2}\left[(\cos T1 - \cos T2) + \frac{1}{2\mu}(\sin T1 - \sin T2)\right] - (z1s\cdot\cos T1 - z0s\cdot\cos T3)\right\} + LNX\left\{\frac{z1s}{2}\cdot\left[\frac{1}{2\mu}(\cos T1 - \cos T2) - (\sin T1 - \sin T2)\right] + (z1s\cdot\sin T1 - z0s\cdot\sin T3)\right\}\right]$$
$$-H_1 \le z < 0 \tag{5.10b}$$

$$\psi' = \frac{Q_o}{Ri}e^{-\pi\mu}\left[TNX\left\{\frac{z1s}{2}\left[\frac{1}{2\mu}(\cos T1 - \cos T2) - (\sin T1 - \sin T2)\right] + (z1s\cdot\sin T1 - z0s\cdot\sin T3)\right\} - LNX\left\{\frac{z1s}{2}\left[(\cos T1 - \cos T2) + \frac{1}{2\mu}(\sin T1 - \sin T2)\right] - (z1s\cdot\cos T1 - z0s\cdot\cos T3)\right\}\right]$$
$$0 \le z \tag{5.10c}$$

where

$z1s = \sqrt{|z|/H_1}$; $z0s = \sqrt{|z|}$; $T1 = \mu\ln(|z|/H_1)$;
$T2 = \mu\ln(H_1|z|)$; $T3 = \mu\ln|z|$; $TNX = \tan^{-1}x - \tan^{-1}x/b_2$;
$LNX = \frac{1}{2}\ln\left[(b_2^2+x^2)/(1+x^2)\right]$

The nondimensional variables are defined by (the tildes are dropped in the above equation)

$$(\tilde{z},\ \tilde{H_1}) = (z/H_o,\ H_1/H_o);\ \tilde{\psi} = \psi'/U_oH_o;$$
$$(\tilde{x},\ \tilde{b_2}) = (x/b_1,\ b_2/b_1);\ \tilde{Q_o} = Q_ogb_1H_o/(c_pT_oU_o^3). \tag{5.11}$$

The total streamfunction has the nondimensional form

$$\psi = \frac{1}{2}(1 - z^2) + \psi'. \tag{5.12}$$

Figure 31 shows the total streamfunction and the vertical velocity for a shear flow with Ri=10, H_1=0.2, and Q_1=0.25. Notice that these parameters

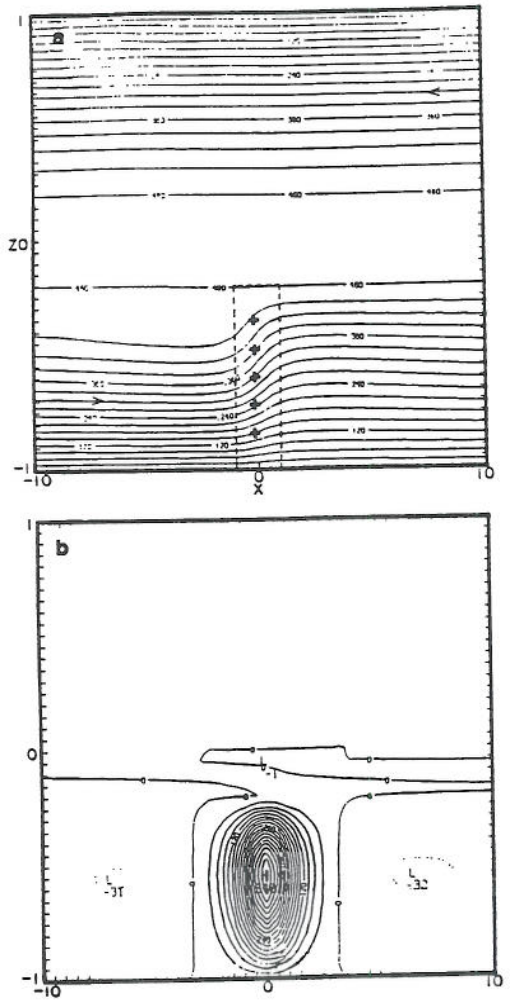

Fig. 31: (a) Streamlines for a two-dimensional shear flow with a critical level (z=0) over an isolated heat source which is concentrated within the dashed lines. The solution is given by Eq. (5.10) with Q_0=0.25, Ri=10, H_1=0.2, and b_2=10. (b) Vertical velocity for (a). Dashed lines indicate negative vertical velocity. (From Lin, 1987)

are nondimensionalized. The corresponding dimensional parameters may be considered as U_0=6.3 m s^{-1}, H_0=2000 m, H_1=400 m, and N=0.01 s^{-1}. The heat source is located below the critical level, z=0. The heating depth is 1.6 km. Below the critical level, a broad region of downward displacement is established upstream of the heat source followed by a region of upward displacement downstream. The vertical motion is almost symmetric with respect to the heating center because the differential advection effect of the basic wind is small due to the prescribed weak shear. On both the upstream and downstream sides of the updraft there exist two weak compensated downdrafts. This response is similar to the motions induced in a quiescent stratified fluid (e.g., Lin and Smith, 1986; Nicholls et al., 1991). Above the critical level, the flow is almost undisturbed because the thermally forced gravity waves are attenuated exponentially as they pass through the critical level. This result is consistent with the free wave solution of Booker and Bretherton (1967) and the mountain wave solution of Smith (1986). Beneath the critical level, the local vertical wavelength decreases as the local horizontal basic wind decreases.

Figure 32 shows a case similar to Fig. 33 except with Ri=1. The corresponding dimensional parameters may be considered the same as in Fig. 33 except with U_0=20 m s^{-1}. The response is significantly different from the previous case. The vertical motion is much stronger than the previous case. A region of a strong downward motion is established upstream of the heating center. The region of maximum upward motion is shifted downstream of the heating region. The broad descent is produced by the compensating downdraft associated with the updraft. Below the critical level, the region of updraft is displaced downwind. This is caused by the advection effect imposed by the basic wind due to stronger vertical shear which now exists as compared with previous case. Near the top of the

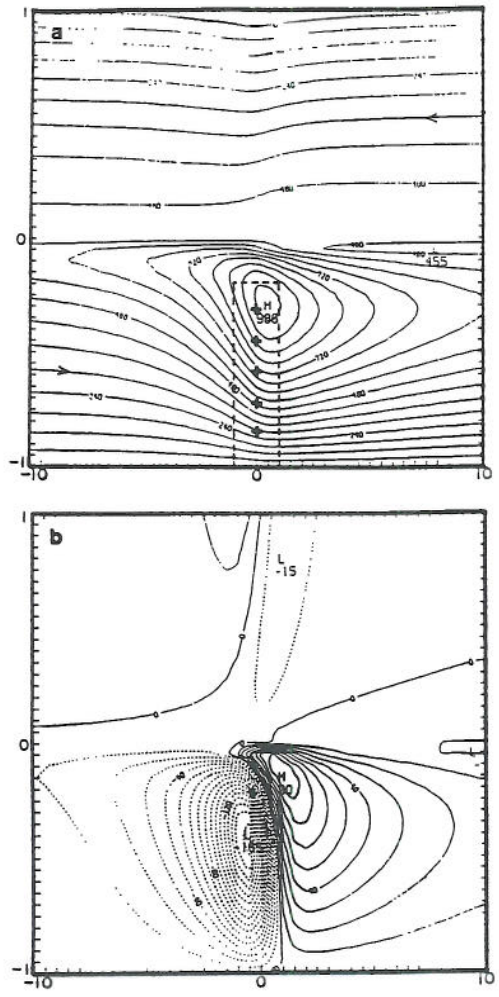

Fig. 32: As in Fig. 31 except with Ri=1. (From Lin, 1987)

heat source, there exists a region of flow recirculation. The thermally forced gravity wave is able to propagate upward to the upper layer above the critical level, although the amplitude is relatively weak. The upstream tiit of the wave in this layer indicates that the wave is able to propagate to infinity. Figure 33 displays the momentum flux for the case of Fig. 32. The momentum flux at the surface is zero as required by the lower boundary

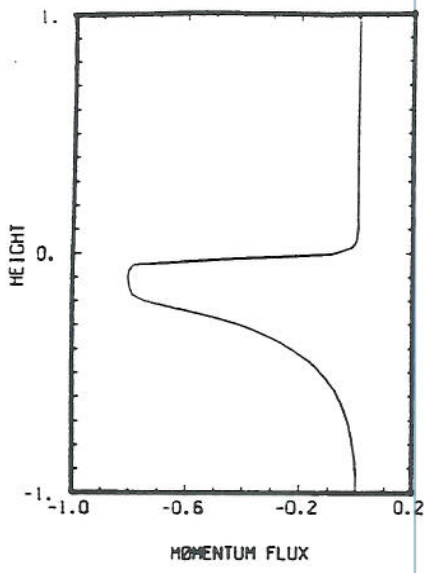

Fig. 33: The vertical momentum flux for the flow field of Fig. 32. (From Lin, 1987)

condition. The momentum flux has a negative value with increasing magnitude in the heating layer, i.e. -1<z<-0.2, and a constant negative value above the heating top until the critical level is reached. This result is consistent with the theory of Eliassen and Palm (1960), which states that the momentum flux does not change with height in a region with no forcing, except possibly at levels where U=0. The vertical flux of horizontal momentum increases almost discontinuously to a small positive value above the critical level as the basic flow reverses its direction and the disturbance is very weak there. The abrupt increase of the momentum flux across the critical level is associated with the absorption of the wave energy by the critical level. The above solution, Eq. (5.10), has been adopted by Crook and Moncrieff (1988) in a study on the effect of large-scale convergence on the generation and maintenance of deep moist convection.

Latent heating always exists in the vicinity of the critical level in a moist convection. The procedure for solving the mathematical problem of a shear flow over an elevated heat source which exists in the vicinity of the critical level is similar to the above case (Lin, 1987). Figure 34 shows the response of a shear flow over an elevated heating in a stratified, unbounded fluid. The existence of thermal forcing in the vicinity of the critical level can modify the flow significantly. In the vicinity of the critical level (z=0), the fluid particle on the left hand side in the lower layer experiences a strong upward motion near the heating center (x=0), crosses the critical level, and then returns to the left of the domain in the upper layer. In addition, the flow near the concentrated heating region is dominated by upward motion, as indicated by Fig. 34b. The consistency of the vertical motion and the heating at the heating base is important in order to support the existing convection. The heating base may represent the cloud base or the top of the moist boundary layer where the surface air becomes unstably buoyant in a cumulus convection (Lindzen, 1974). The vertical motion in the vicinity of the critical level may be explained by inspecting the thermodynamic equation [Eq. (3.4)]

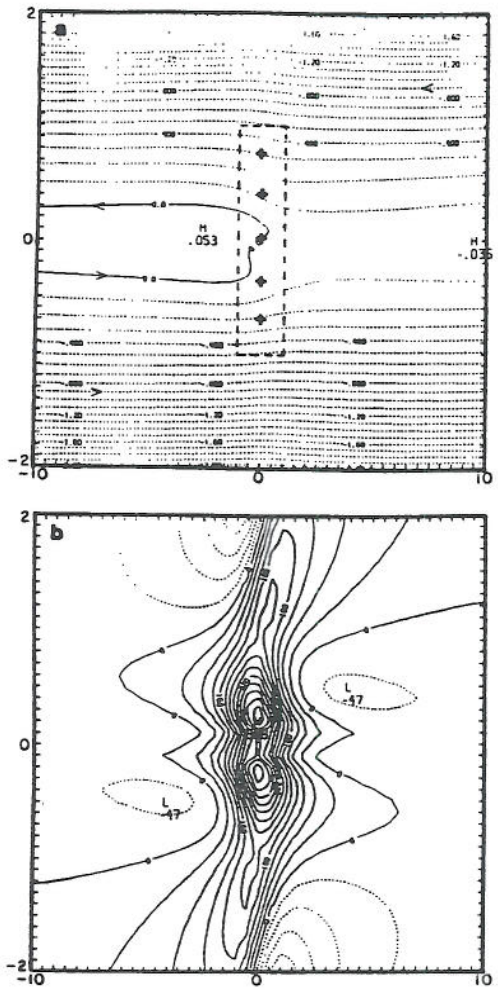

Fig. 34: (a) Streamlines for flow over an isolated heat source in an unbounded continuously stratified fluid. The heating is concentrated in the region enclosed by dashed lines. (b) Vertical velocity for (a). The Richardson number associated with the basic flow is 1. (From Lin, 1987)

$$U\frac{\partial \theta'}{\partial x}+\frac{N^2\theta_o}{g}w'=\frac{\theta_o}{c_pT_o}q' \qquad (5.13)$$

The above equation may be approximated by

$$w'=\frac{g}{c_pT_oN^2}q' \qquad (5.14)$$

in the vicinity of the critical level since U=0 there. This indicates that the vertical velocity near the critical level is proportional to the heating rate. Since the flow structure resembles that asscociated with a midlatitude squall line, one may conclude that the condensational heating in the vicinity of the critical level plays an important role in the interaction of the flow below and above the critical level.

Lin and Chun (1991) solved a similar problem analytically for a flow over a low-level heat sink and

obtained a result similar to that of Lin (1987). From a scale analysis of the governing equations, a nonlinearity factor of the thermally induced finite-amplitude waves $gQ_o b_1/(c_p T_o U_o^2 N)$, is found. The symbol U_o denotes the basic wind at the surface. This factor reduces to that found by Raymond and Rotunno (1989) for the uniform flow case. Using a simple nonlinear model, Lin and Chun (1991) found that the hydrostatic response of a shear flow with a critical level to a steady cooling can be categorized as either a stationary cold pool, or a density current, depending upon the strength of the effective cooling. For a small Richardson number flow, the cold pool is stationary with respect to the upstream flow because most of the cooling is used to compensate the positive vorticity generated by the positive wind shear (Fig. 35a). In this case, the response is similar to the linear steady state case (Fig. 3a of Lin and Chun, 1991). For a large Richardson number flow, the cold pool is able to propagate upstream because the effective cooling, which increases with time, is strong enough to push the outflow against the basic wind (Fig. 35b). It is interesting to observe that internal gravity waves are produced and propagate upward at the head of the density current. Similar results also are obtained by Chen et al. (1992) in a nonhydrostatic numerical simulation of gravity currents. From the comparison between linear theory and nonlinear model results, it is found that the nonlinearity appears to reduce the wave disturbance in the layer between the critical level and the cooling top, while it tends to strengthen the density current or cold pool near the surface.

As mentioned in Section 4, Lindzen and Tung (1976) proposed that a stable wave duct adjacent to the surface may exists if it is capped by an unstable layer which contains a critical level. Chun and Lin (1992) have investigated the steady response

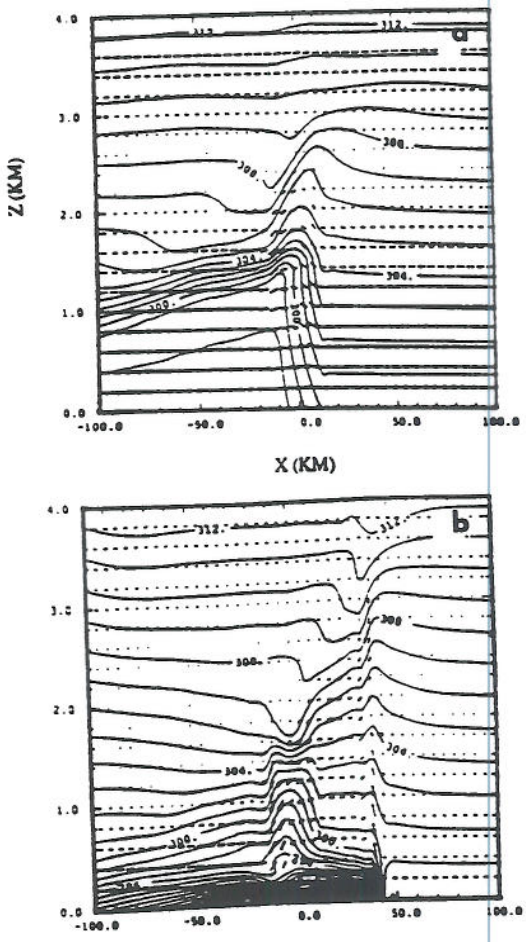

Fig. 35: Potential temperature fields for a two-dimensional, hydrostatic, continuously stratified shear flow with a critical level (z=2.5 km) over a steady heat sink (b_1=10km, z≤1.5 km) for (a) Ri=0.69 and U_o=30 m s^{-1}, (b) Ri=6.25 and U_o=10 m s^{-1}. The basic wind blows from right to left in the lower layer (z≤2.5 km) and reverses its direction in the upper layer. Notice that an upstream propagating density current develops in the large Richardson flow. (From Lin and Chun, 1991)

analytically in the same type of environment but with a diabatic cooling in a three-layer atmosphere. The